Ocean circulation and sea-ice distribution changes induced by an increased melting rate under the Filchner-Ronne Ice Shelf

Author:
Cătălin Paţilea

Supervisors:
Prof. Dr. Thomas Jung
Prof. Dr. Torsten Kanzow

University of Bremen
September 10, 2014

Abstract

The Finite Element Sea-ice Ocean Model (FESOM) is being utilized with a high resolution mesh focused on the Antarctic marginal seas and ice shelves to investigate the changes induced in ocean circulation and sea ice distribution by prescribing increased melt rates for the Filchner-Ronne Ice Shelf (FRIS). The increased freshwater received by the Weddell Sea leads to higher stratification, reducing convection and leading to less freshwater reaching the bottom layers. Sea ice distribution changes in the Weddell Sea with higher concentration and thickness along the peninsula during summer while during winter maximum, sea ice volume is increased over a large area in the Weddell Sea. Increased surface freshening and water column stability inhibits convection which reduces the Weddell Gyre transport and increases bottom layer potential temperature, bringing down Antarctic Bottom Water formation.

Acknowledgements

I want to thanks my supervisors Thomas Jung and Torsten Kanzow for their continuous guidance during my fight with the unknowns of research. I want to give special thanks to Ralph Timmermann for his constant help which moved me forward with my project and his assistance in establishing the initial conditions of my experiments and solving all the technical problems related to them. I would also like to thanks my collegue Madlen Kimmritz for advice and her very useful MOC tool, Dmitry Sidorenko, Martin Losch and Sergey Danilov for answering my pestering questions. And finally I would like to thanks AWI for giving me the opportunity to work on an interesting subject in a very nice and pleasant environment.

Contents

1 Introduction

1.1 Background

Climate defines life on our planet. It influenced how plants and animals evolved and also shaped how humans adapted to the specific regions. It is imperative to study the climate since it is greatly related to human welfare around the globe by directly influencing human activities or by indirect changes to the surrounding biosphere.

Climate research has seen great improvements in the last decades. Satellites have increased the area coverage and frequency of measurements in addition to larger sets of paleodata. This increase in data helped to better understand the physics behind climate and led to the development of more accurate climate models.

Climate change is defined in the fifth IPCC report (T.F. Stocker, 2013) as "a change in the state of the climate that can be identified by the change in the mean and/or the variability of its properties and that persists for an extended period of time". The global average land and sea surface temperature increase in the period $1880 - 2012$ is 0.85K. Also due to new devices like the Argo floats we now have a network for an almost continuous observation of the ocean. In the last four decades, an increase of the temperature and heat content at all depths has been observed Fig. 1. Although paleodata show that Earth has been warmer in the past and had higher concentrations of greenhouse gases, in the last 800,000 years the concentration of CO_2 and CH_4 where constrained between certain thresholds which now have been surpassed.

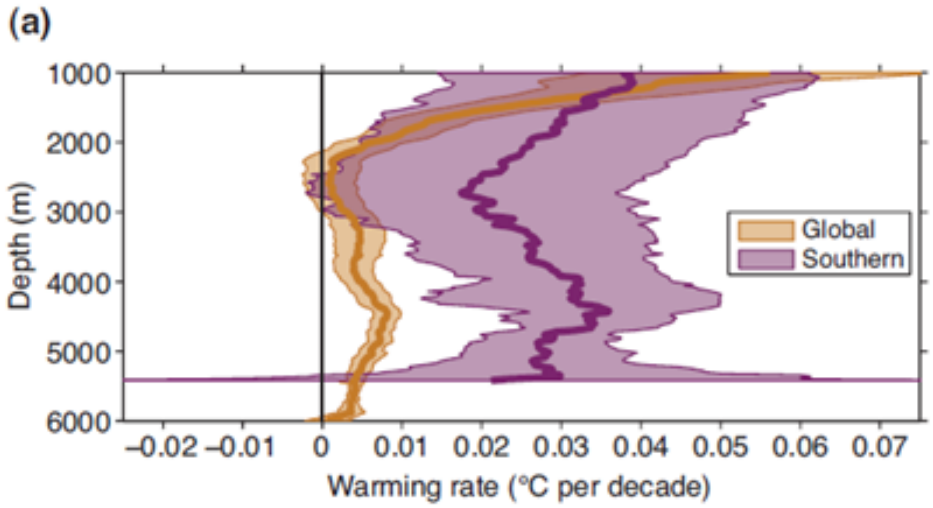

Figure 1: Areal mean warming rates (°C per decade) versus depth with 5-95% confidence limits centered on 1992-2005 period for the whole ocean (orange)and for the Southern Ocean (purple)(T.F. Stocker, 2013)

One area of importance affected by climate change is the Antarctic region. It contains

70% of the planet's freshwater reserves in the ice sheet and ice shelves, it influences the global energy budget through the albedo effect and has the potential of rising the global sea level by 60 meters due to melting. During the southern hemisphere winter, sea ice develops around the continent and covers at its maximum $2 \cdot 10^6$ km^2, an area larger than the Arctic sea ice maximum. Another trait of the Antarctic sea ice is that it is thinner and multi-year ice covers a small surface, usually in the Weddell Sea close to the ice shelf. Also Antarctic sea ice (especially in the Weddell Sea and Ross Sea sectors) is responsible for the creation of the Antarctic Bottom Water (AABW), the coldest and densest water mass which drives global circulation and is important for ventilation of the deep ocean.

The Antarctic has warmed overall since the 1950s but there is low confidence in the magnitude and its spatial distribution (T.F. Stocker, 2013). For the Southern Ocean it has been observed an increase in temperature of 0.03℃ per decade south of the Sub-Antarctic Front with a reduction in transport of 8.2 Sv for the AABW, while in the Weddell Sea the temperature increased by 0.015℃ per decade for the period 1984-2008. The salinity for the first 1000 meters of the Southern Ocean has decreased by 0.01 per decade in the period 1980-2000 more than any other regional change.

The Antarctic Ice Sheet recorded mass loss in the last two decades due to melting and iceberg calving (T.F. Stocker, 2013). Since the ice sheet drains into the ice shelves which serve as buttresses for the ice flow, changes in the basal melting of ice shelves is extremely important to the loss rate of mass from the ice sheet. The cyclonic gyre in the Weddell Sea may allow Circumpolar Deep Water to enter from the east into the Filchner-Ronne Ice Shelf cavity, bringing the warmer water of approximately 0.9℃ at the Greenwich meridian to the front of the ice shelf at -1.5℃ despite the continental slope. This warm water mass doesn't advance deep into the cavity but the high salinity shelf water formed here that is the main driver of sub-cavity circulation brings this heat to the shelve's grounding line. One hypothesis assumes that rising sea surface temperatures inhibits the formation of sea ice and the resulting high density water so in the end reducing the heat transfer to the grounding line. But in the same time less sea ice concentration and thickness increases sea ice drift speed and a more efficient transfer of momentum to the ocean surface off the Luitpold coast, coupling this with the warmer water in a global warming scenario actually rises temperature in the cavity by 2℃ increasing the basal melt rate from 0.2 meter/year to 4 meters/year (H.H. Hellmer, 2012). The Filchner-Ronne Ice Shelf is the biggest ice shelf by volume and according to R. Timmermann (2013) due to a decrease in salinity on the continental shelf and the intrusions of the mentioned warm deep water under the cavity, FRIS may become the biggest contributor of total ice shelf basal mass loss in the 22^{nd} century with an increase of the basal melting by a factor of 10 by 2150 from the present value of approximately 90

Gt/year. In the H.H. Hellmer (2012) experiment the Ross Ice Shelf's basal mass loss remains constant during the twenty-second century at around 80 Gt/year, while in R. Timmermann (2013) although delayed, the basal mass loss starts to increase reaching 500 Gt/year by 2150. Even though we observe increased basal melt rates for the smaller ice shelves none of them increases as big as FRIS. Their grounding lines are not as deep so their melting is less correlated with changes in ocean circulation and more of a direct effect of surface temperature increase (R. Timmermann, 2013).

Due to this possible increased melting it becomes important to try to isolate and analyze the climate signal of the freshwater flux from the Filchner-Ronne Ice Shelf. To obtain this separation we are using a sea-ice ocean model that after initialization is separated into two branches for comparison. For the first (reference) branch the model computes the melt rates for FRIS normaly, by taking into account the ice-ocean interface salinity, temperature and heatfluxes.While for the second (enhanced) branch, the melt rates for FRIS were prescribed using much higher values. By comparing the output of the two model runs we can observe changes that are a direct result from the freshwater flux. By using this test case we eliminate the feedback from the higher temperature oceans, changing wind patterns and precipitation from the future projection. Although the high melt rates come from a much warmer ocean and are not realistic in the present day conditions, this can be treated as a conceptual simulation that will help us understand better, future results from projections.

1.2 Ice Shelves

Ice shelves are ice sheet or glacier extensions over the water and appear just around the shores and in the bays of Antarctica, Greenland and Ellesmere Island in the Canadian Arctic. They usually rise at least 2 meters over the water and can be from 100 meters thick to over 1000 meters. The area where the floating ice meets resting bedrock is called grounding line. The creation of ice shelves is done by accumulation of snow over the ice sheet/glacier surface which pushes ice away from the point of accumulation and towards the sea. Away from the grounding line we also have another mechanism which helps growth which is the freezing of water at the base of the ice shelve but this is mostly a mechanism for glaciers. Ice shelves mainly loose mass through two known processes, basal melting and ice calving. Large ice shelves with long grounding lines produce dome shaped ice rises while smaller ones can have irregular shapes (K. M. Cuffey, 2010).

The Antarctic continent is surrounded by ice shelves (Fig. 2), 18,877 km representing 42% of the total of 45,317 km of coastline. Also the ice shelves collect 20% of the snowfall over the Antarctic. The two biggest ice shelves are found in the Antarctic with the Ross Ice

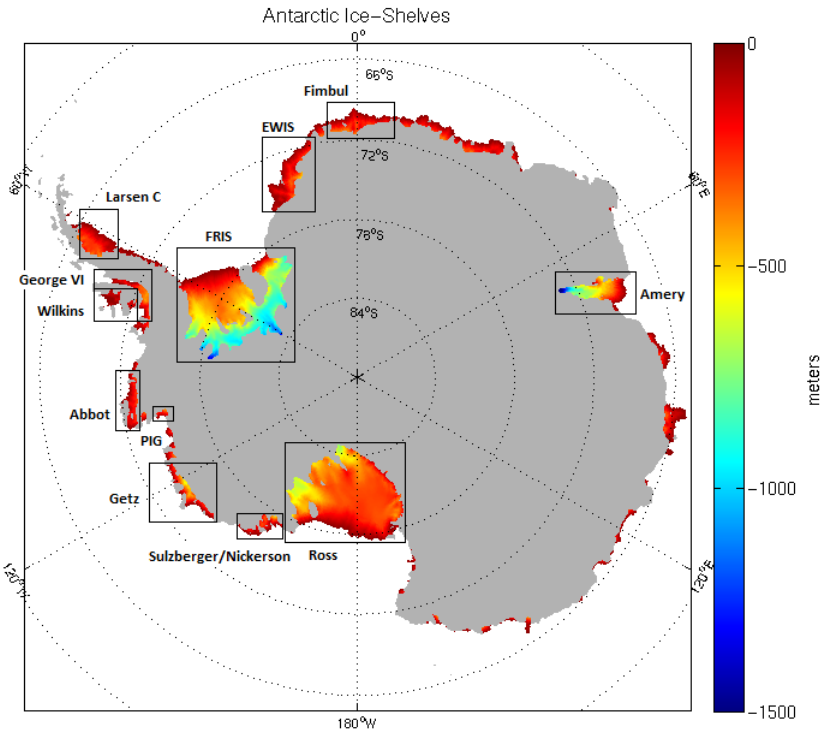

Figure 2: Reprezentation of the ice shelves included in the model and their ice bottom depth (meters)

Shelf being the biggest by area with approximately $470 \times 10^3 km^2$ while the Filchner-Ronne Ice Shelve is approximately $433 \times 10^3 km^2$ but the ice reaches close to 2100 meters below sea level close to the grounding line (E. Rignot, 2013) making FRIS the highest in volume. The big ice shelves lose mass at the ice front through calving but also experience basal melting and freezing. Most smaller ice shelves lose mass through iceberg calving and less to basal melting. While basal melting releases freshwater locally, in the case of calving, the icebergs are transported away from the point of calving by ocean currents, wind and can get locked in sea ice and be moved together with it. This way they become a moving source of freshwater, spreading the plume directly over a larger area and freshening mostly the surface waters.

Also simulations (Hellmer, 2004) show that the meltwater plumes from the ice shelves stabilize the water column in front of the them but also downstream due to advection. This leads to less vertical exchange and reduces heat transfer to the surface which leads to colder and fresher shelf waters and thicker sea ice.

One important role of the ice shelves is buttressing. In our case this means that for an ice

sheet the surrounding ice shelves stabilize the ice flow at the grounding line. So a shrinkage or removal of an ice shelf can increase the ice flow in the ocean (T. K. Dupont, 2005) as seen in Fig. 3, destabilize the ice sheet and maybe lead to its disintegration and to sea-level rise. Several smaller ice shelves have disintegrated already in the West Antarctic and Antarctic Peninsula, like the Larsen A and B ice shelves in the Weddell Sea in 1995, respectively 2002, the Jones Ice Shelf, Müller Ice Shelf and Wordie Ice Shelf, in 2003, 2008, respectively 2009, along the western coast of the Antarctic Peninsula. Also it has been observed (E. Rignot, 2014) that there is a increased grounding line retreat of the Pine Island, Thwaites (I. Joughin, 2014), Smith and Kohler glaciers in West Antarctica in the last decade and an increase of 77% ice discharge in the Amundsen Sea Embayment (J. Mouginot, 2013) compared to 1973 possibly revealing increased instability of the West Antarctic Ice Sheet (WAIS). In case of disintegration WAIS can contribuite with an eustatic sea-level rise of 3.3 meters with big regional variations (J.L. Bamber, 2009).

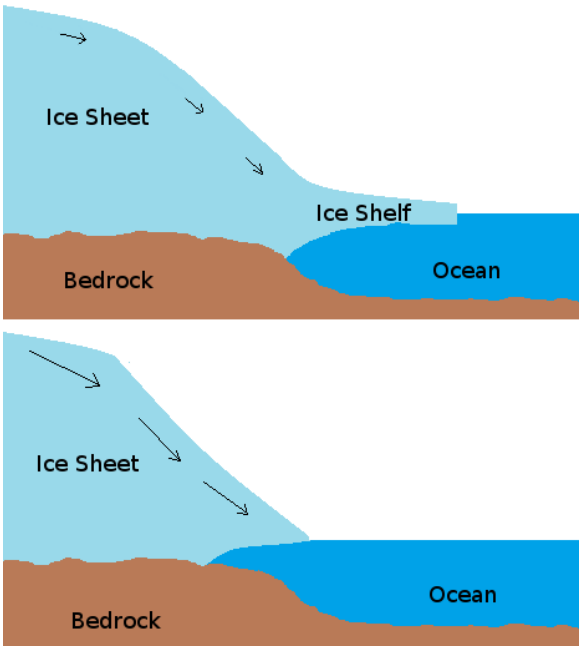

Figure 3: Reprezentation of ice shelf buttressing role for the ice flow of the ice sheet into the ocean

The Filchner-Ronne Ice Shelf which is the main focus of this thesis is located south of the Weddell Sea in the Atlantic sector of the Southern Ocean. It's surrounded by the Antarctic Peninsula and Ellsworth Land in the west, Coasts Land in the East and the Weddell Sea in the north. The Filchner-Ronne Ice Shelf is actually composed of two ice shelves, the Filchner Ice Shelf in the eastern side and the smallest of the two and the Ronne Ice Shelf in the west. They are separated by the Berkner Island and are joined together at its southern tip. West of the Berkner Island are the Henry and Korff Ice Rises. Although all three have

their actual rockbeds underneath the sea level they form barriers under the ice shelf and shape the sub-cavity circulation.

The main ice fluxes into the ice shelf from are the Evans and Rutford Ice Streams and through the Carlson Inlet in the west, flowing away from the Antarctic Peninsula and West Antarctic Ice Sheet, the Institute, Foundation, Academy and Support-Force Ice Streams in the south and Bailey, Slessor and Recovery Ice Streams in the east coming from the East Antarctic Ice Sheet.

As it can be seen in Fig. 2 the ice draft depth for FRIS increases with distance from the ice front, reaching a mean of 800 meters behind Berkner Island and the two ice rises and reaching well below 1000 meters at the grounding line of the Rutford and Foundation Ice Stream.

1.3 Basal melting modes

Basal melting accounts for more mass loss in the Antarctic than for calving (E. Rignot, 2013) with 1325±235 gigatons per year (Gt/year) while the estimate for calving is 1089±139 Gt/year. Thus the study of basal melting is important for understanding future ice sheet flow and mass balance and sub-cavity ocean circulation.

There are three known modes of basal melting related to ocean circulation (S. S. Jacobs and Frolich, 1992) as seen in Fig. 4 . The main mode represents the melting in the deep areas of the cavities close to the grounding line which transforms dense shelf water into the cold and fresh Ice Shelf Water (ISW). The ISW is mainly formed during winter due to the sea-ice formation at the sea surface. This process eliminates brine which mixes with under sea-ice water and starts downwelling. The continental shelf usually deepens towards the grounding line thus the denser water is guided towards the lower section of the ice shelf. Due to the fact that sea-water's freezing/melting temperature decreases with depth, the shelf water that came from the surface will be with as much as 1℃ warmer that the in-situ melting temperature thus a melting. This process provides a flux of freshwater which decreases the salinity and temperature initiating a thermohaline convection driving the shelf water upwards along the sloped cavity and transforming it into a relatively fresher but much colder ISW. Some of the water refreezes along the way forming marine ice but the melting exceeds the refreezing and this mode is the main exporter of melted water out of the cavity (S. S. Jacobs and Frolich, 1992). This is the main mode of mass loss for the bigger shelves while the smaller shelves have a higher variability including net freezing from this mode.

The second mode represents the melting done by warm water inflow at intermediate depth from the slope front region. This mode can achieve high rates of melting but can be

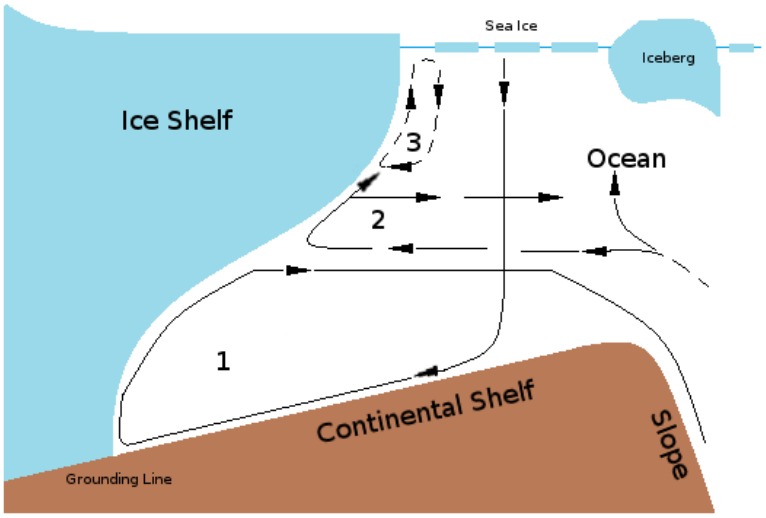

Figure 4: Schematics of the three basal melting modes of an ice shelf, (1) represents the first mode of melting, with high salinity water formed from sea ice, goes down the shelf slope to the grounding line where it melts the ice shelf, (2) second mode of melting representing warm water inflow underneath the ice shelf at intermediate depth, (3) represents ice front melting (S. S. Jacobs and Frolich, 1992)

limited in area and a large part of the heat can be drawn to the surface and not reach the ice-water boundary. In most cases the source for heat in the Antarctic for the second mode is the Circumpolar Deep Water. One ice shelf in which this is the main mode is the George VI Ice Shelf but it also seems to be a factor in the disintegration of the Wordie Ice Shelf (S. S. Jacobs and Frolich, 1992).

The third and last mode of melting appears at the and underneath the ice front within the first 100 km and it's done by tidal pumping and by seasonal warm waters and this results in a high regional variability of melting.

1.4 Weddell Sea

The Weddell Sea is positioned in Atlantic sector of the Southern Ocean, and it is bounded to the south by the Filchner-Ronne Ice Shelf, the Antarctic Peninsula with Joinville Island to the west, while the eastern limit is close to 20°W. The most important component of the Weddell Sea is the cyclonic Weddell Gyre which actually extends more, reaching South Scotia, the North Weddell and Southwest Indian Ridges in the north and getting to 30 to 40°E (E. Fahrbach, 2001). The Weddell Gyre moves 50 Sv of water over the Greenwich Meridian while between the tip of the Antarctic Peninsula and Kapp Norvegia the gyre transports 29.5 Sv.

Concerning water masses in this area, we have the Circumpolar Deep Water (CDW) at the north edge of the Weddell Gyre, with Antarctic Surface Water above it and the cold

and dense Antarctic Bottom Water beneath. The CDW enters the gyre at the northern and eastern boundaries and mixes, becoming the cooler and fresher Warm Deep Water (WDW) (K. W. Nicholls, 2009). Beneath the WDW we find the Weddell Sea Deep Water which represents the Weddell Sea's component of the Antarctic Bottom Water. A large part of it comes from the east, but there's also some formed at the continental margins and some of the Weddell Sea Bottom Water (WSBW) which is very dense and can't escape the Weddell Basin is upwelled and mixed helping form this water mass. As said before at the top we find the Antarctic Surface Water which cools during the winter, forming sea ice and releasing brine which increases the mixed layer depth and forms the more saline Winter Water. During the Antarctic summer when the sea ice is melting the Winter Water is freshened and the water column is returned to a stronger stratification state(K. W. Nicholls, 2009).

The formation of Antarctic Bottom Water is very important due to its importance in creating a downwelling area in the Southern Ocean and participating in as a bottom water mass in the Meridional Overturning Circulation. The AABW is mostly formed during the long Antarctic winter when temperatures are extremely low and katabatic winds are blowing from the continent towards the sea, removing heat from the coastal shelf waters generating sea ice. Although sea ice insulates the ocean from further heat loss, the strong winds move the sea ice away from the coast and from the place of origin, exposing the ocean again and renewing the cycle. During sea ice formation, salinity in the surface layer increases over 34.6 PSU so the water becomes dense enough to sink. This water goes down the slope beneath the ice shelf towards the grounding line. Together with depth, the freezing point of sea water decreases so that the warm shelf water put in contact with the ice shelf can reach temperatures below -2℃. Due to melting the water is becoming much colder and slightly fresher and is advected along the ice shelf slope transforming into Ice Shelf Water, flowing over the dense shelf water entering the cavity. Once passing over the continental slope it descends into towards the abyssal plain and due to compressibility of sea water, its density increases and transforms into AABW.

1.5 Meridional Overturning Circulation

The Meridional Overturning Circulation (MOC), also sometimes called the Global Conveyor Belt, represents the usual movement of warm surface waters from the equator towards the poles where they cool down, sink and generate dense deep waters which continue moving towards the equator (Dirk Olbers, 2012) ventilating the deep ocean. Most of the circulation is driven by density differences due to the changes in temperature and salinity of the moving water masses induced by heat and freshwater flux exchange mainly at the surface. This com-

ponent of the MOC is called the Thermohaline Circulation (THC). The second component is generated by wind-driven major current system like the Gulf Stream and the Antarctic Circumpolar Current (ACC).

A simple view of this system starts with the downwelling of water in the Arctic due to low temperatures and brine emission during the formation of sea ice. The water mass moves southwards along East coast of the American continent. Then in the South Atlantic joins the ACC traveling eastwards and then north, upwelling in the North Pacific. From here it moves southwards passing the Equator and then westwards through the Indian Ocean and south of the African continent. In the Atlantic it starts moving northwards along the eastern coast of the American continent forming the Gulf Stream ending in the Arctic, closing the cycle (Fig. 5). Although this is an extreme oversimplification of the actual water mass movement in the oceanic system, it still gives a general view of the large scale meridional transport.

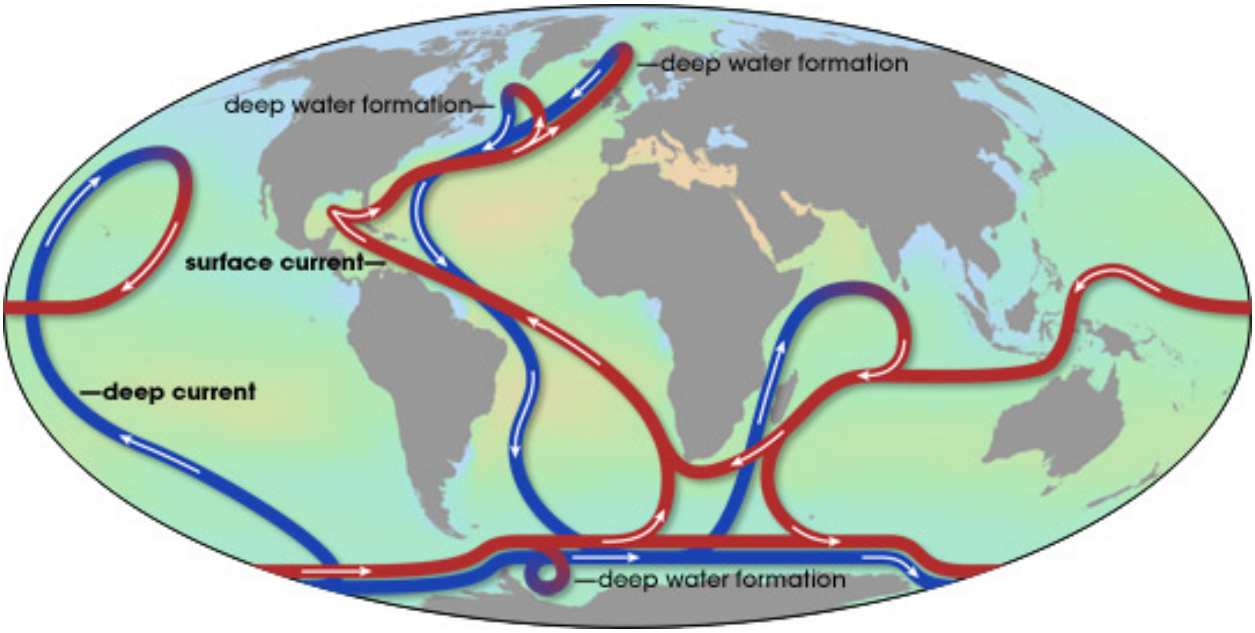

Figure 5: Schematic of the Meridional Overturning Circulation, with warm surface currents in red and cold deep currents in blue (source NASA website)

As seen in Fig. 5 the two main downwelling regions are the in the North Atlantic, mainly the Greenland Sea and Labrador Sea where the North Atlantic Deep Water (NADW) is formed and in the Southern Hemisphere, in the Ross and Weddell Sea where the Antarctic Bottom Water is formed. Although the heaviest water at formation is the NADW, because of its compression with sinking, the AABW remains the coldest and densest water that fills the deep basins.

2 FESOM Model

2.1 Model description

For this study we used the Finite Element Sea-Ice Ocean Model (FESOM) based on an earlier finite element model (S. Danilov, 2009) that was developed at the Alfred Wegener Institut (AWI). The model divides the ocean thermo-hydrodynamics equations in two groups that will be resolved separately. The dynamic part solves the momentum equations:

$$\partial_t \mathbf{u} + f(\mathbf{k} \times \mathbf{u}) + g\nabla\zeta - \nabla \cdot A_l \nabla \mathbf{u} - \partial_z A_v \partial_z \mathbf{u} = -\frac{1}{\rho_0}\nabla p + \mathbf{F}_u \tag{1}$$

using the integral continuity constraint

$$\partial_t \zeta + \nabla \cdot \int_{z=-H}^{z=\zeta} \mathbf{u} \mathrm{d}z = 0 \tag{2}$$

and the hydrostatic balance

$$\partial_z p = -g\rho \tag{3}$$

where $\mathbf{u}$ is (u, v) and together with w represent the velocity vectors, f is the Coriolis parameter, k represents the vertical unit vector, g is the gravitational acceleration , ζ is the sea surface elevation, A_l represents the lateral momentum diffusion coefficients while A_v represents the vertical one. ρ and ρ_0 represent the density variation, respectively the mean sea density and $\mathbf{F}_u$ is the non-linear advection.

The thermodynamics part solves the continuity equation for the vertical velocity w

$$\partial_z w = -\nabla \cdot \mathbf{u} \tag{4}$$

tracer evolution equations

$$\partial_t C^m + \nabla \cdot (\mathbf{u} C^m) + \partial_z (w C^m) - \nabla \cdot K_l^m \nabla C^m - \partial_z K_v^m \partial_z C^m = 0 \tag{5}$$

and calculates density by using the equation of state

$$\rho - \rho(T, S, p) = 0 \tag{6}$$

where C^m is the m-th tracer and K_l^m and K_v^m are the lateral and vertical diffusion coefficients for the respective tracer. These basic systems can't be solved analytically so they are discretized spatially and temporally.

The surface grid is unstructured and constructed from variable size triangles, while the

three dimensional elements are built by cutting prisms underneath the triangles using horizontal triangles in the upper layers and terrain following triangles in the lower layers (Fig. 6). The resulting prisms are then divided in elementary tetrahedrals. This feature allows the meshes to have high resolution in the areas of interest or in places with higher resolution requirements like coasts, straits and islands while lowering the resolution in other areas to reduce the computational burden.

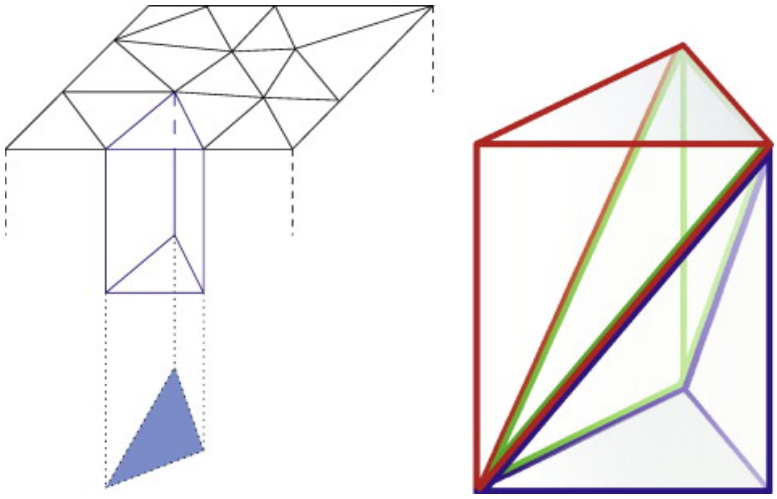

Figure 6: Reprezentation of the unstructured mesh used by FESOM. On the left, the horizontaly alligned first layer elements are represented with the terrain follwing one close to the bottm. On the right, the division of the prism element into tetrahedra (R. Timmermann, 2009)

The model has implemented a finite element sea ice model with both dynamics and thermodynamics included. The growth of sea ice is computed by taking into account sensible and latent heat fluxes, incoming shortwave and longwave radiation, heat flux to the mixed layer from the deeper ocean and black body radiation of the surface water. A prognostic snow layer is implemented while the heat storage in both the snow layer and the ice layer is not considered, simplifying the temperature profiles to linear ones. For sea ice dynamics, the model includes a elastic-viscous-plastic rheology which accounts for ice-ocean and ice-atmosphere interaction and internal stresses.
The ice shelf component (R. Timmermann, 2012) uses a system of three equations to resolve the basal melting rate and temperature and salt in the sea water and ice boundary layer (David M. Holland, 1999). The system determines the freezing point of seawater:

$$T_B = aS_B + b + cp_B \tag{7}$$

and considers heat conservation

$$Q_I^T - Q_T^M = Q_{latent^*}^T \tag{8}$$

$$Q^T_{latent^*} = -\rho_M w_B L_f \tag{9}$$

and salt conservation

$$Q^S_I - Q^S_M = Q^S_{brine^*} \tag{10}$$

$$Q^S_{brine} = \rho_M w_B (S_I - S_B) \tag{11}$$

where T_B and S_B are temperature and salinity at the ice-ocean interface, a, b and c are empirical constants, p_B is the pressure at the interface, Q^T_I and Q^T_M represent the conductive heat flux through the ice shelf and the diffusive heat flux in the boundary layer, while $Q^T_{latent^*}$ represents the latent heat at the ice-ocean interface,with $\rho_M w_B$ being the mass of melting or frozen ice, L_f is the latent heat of fusion, Q^S_I and Q^S_M are the salt fluxes through the ice shelf and boundary layer, $Q^S_{brine^*}$ is the salt flux at the ice-ocean interface and S_I and S_B are the bulk salinity of ice shelf and salinity at ice-ocean interface.

The atmosphere is represented as a forcing field with data resulted from other models' output like the Hadley Center Climate Model (HadCM3) or from reanalysis datasets like NCEP/NCAR reanalysis 1.

2.2 Bathymetry

Since we need a detailed representation of the ice shelves cavity geometries for an accurate computation of the melting and freezing rates and sub-ice shelf circulation the RTopo-1 data set(ref RTopo-1) has been chosen for this. It consists of the bedrock topography of the ocean (Fig.7), surface and under the ice sheets and ice shelves; surface elevations representing the bedrock elevation for ice-free continent and ice surface height for ice sheets and ice shelves; ice base topography which has the same value as the bedrock topography over continents but represents the ice shelve cavities over the ocean; masks to identify the components of the data set and finally locations of coasts and grounding lines. Most of the data comes from the S-2004 1-min global bathymetry (a mix of gravimetric and ship-based echo-sounding data) which covers most of the World Ocean. But for the Southern Ocean where the satellite data is scarce the BEDMAP data set has been used and interpolated with previous data.

For some of the ice shelves (Filchner-Ronne Ice Shelf, Larsen, Amundsen Sea, Bellingshausen Sea, Amery and Fimbul ice shelves) newer data has been incorporated. Errors in the ice shelves' ice draft come from firn correction, ice surface errors and deviation from the hydrostatic assumption near the grounding line. The Filchner-Ronne Ice Shelf data which is of interest has a ice thickness error less than 25 meters for most of the ice shelf with possible higher errors close to the grounding line while for the other less densely surveyed ice shelves the errors could be even higher.

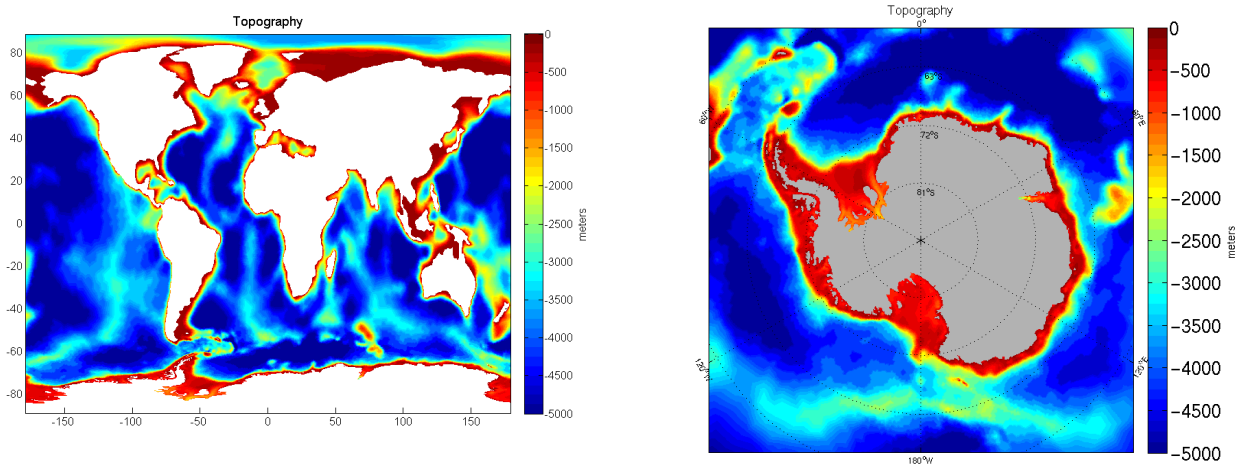

Figure 7: Global (left) and Southern Ocean (right) bathymetry (meters) used in the simulations, derived from the RTopo-1 dataset

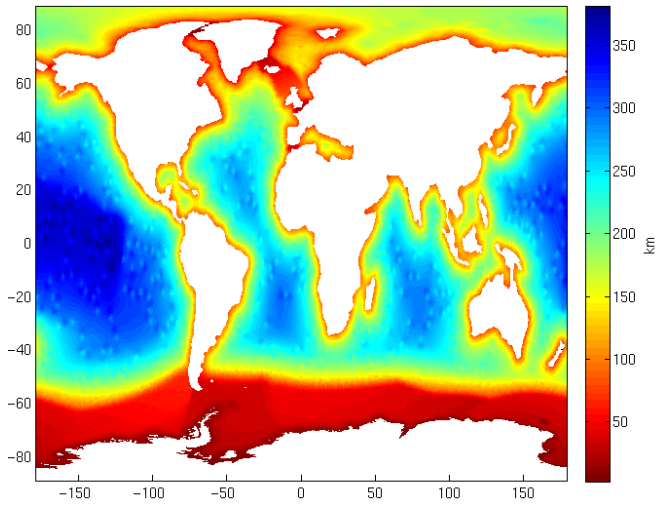

Figure 8: Global mesh resolution (km) map used in the FESOM simulation

The RTopo-1 data set has been used with a mask to cover continental surfaces. In the current setup the mesh has a horizontal resolution of 250-300 km in the large oceanic basins, 50 km near the coasts outside Antarctica. In the southern hemisphere after 50° S the resolution increases getting to 30-40 km for the Southern Ocean, 10 km for the Antarctic coast as seen in Fig. 8 and 7 km under the large ice shelves (Ross Ice Shelf and Filchner-Ronne Ice Shelf). The smaller shelves get to a resolution under 4 km (R. Timmermann,

2013) as seen in Fig. 9. For vertical representation 37 z-levels are used.

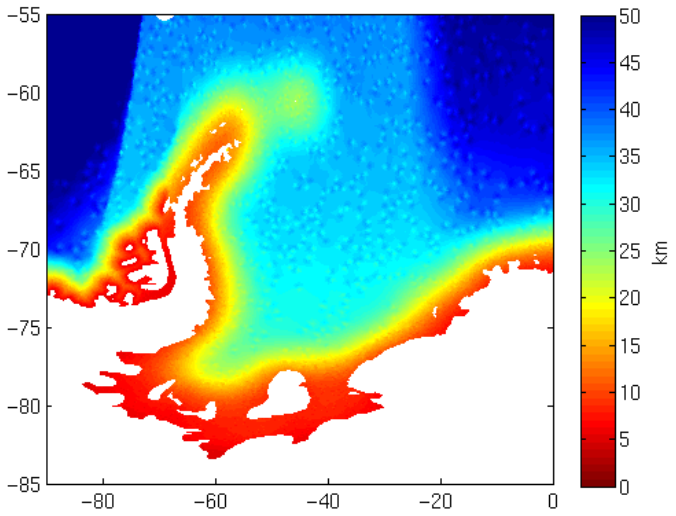

Figure 9: Weddell Sea and surroundings mesh resolution (km) map used in the FESOM simulation

2.3 Model configuration

The surface mesh has a total of 76636 nodes, with just 8194 for the Northern Hemisphere and the rest of 68442 for the Southern Hemisphere, from which, over a third are cavity nodes. The total number of mesh nodes is about $1.8 \cdot 10^6$.

The model's ocean temperature and salinity are initialized with data from the World Ocean Atlas 2001 (WOA2001) and are extended underneath the ice shelves through inter-/extrapolation (R. Timmermann, 2001). The model is forced with daily data from the NCEP/NCAR reanalysis for the period 1958-2010. The model computes shortwave and longwave radiation, turbulent latent and sensible heat fluxes and surface wind by using the $10m$ wind, $2m$ air temperature, specific humidity, total cloudiness and net precipitation.

The period 1958-1979 is used for an initial adjustment of the model. From 1980 the model is split in two, with one reference branch and one enhanced melting branch. The reference branch (which will also be referred as RE) continues computing melting rates for the FRIS dependent on the heat and salinity fluxes at the boundary layer between the ocean and the ice shelf. In the second branch simulation (referred as Enhanced or PE), we prescribe constant melt rates for the FRIS (Fig. 10). The melt rates were obtained from the HadCM3-A1B forced experiment of R. Timmermann (2013) by applying a 10-year average for the 2140-2149. They are kept constant throughout the year. For getting an extended dataset the atmospheric forcing from the 1960-2010 period has been reused in the

continuation of the original simulations. This means that the 2011-2059 period represents the continuation from 2010 of the evolution of the ocean/sea-ice component of the model, but reuses past atmospheric forcing.

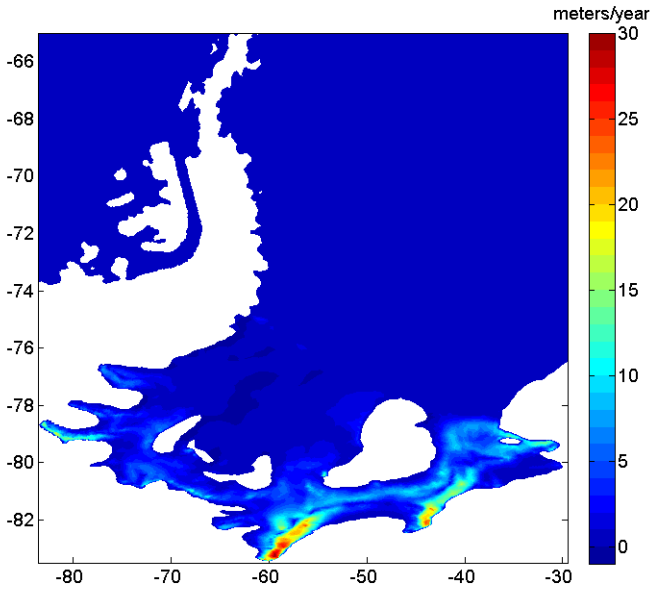

Figure 10: Map of yearly melt rates (meters/year) of the Filchner-Ronne Ice Shelf used for prescribing the enhanced simulation

3 Results

3.1 Basal mass loss

All ice shelves

The total mean basal melting rate for all the ice shelves (Fig.11) in the Antarctic in the RE run is 1128.9 ± 99.3 Gt/year. The maximum value for melting appears in 1980 with 1316.5 Gt/year while the minimum of 951.2 Gt/year is reached in 2001. For the PE simulation where the prescribed total basal melting rate of 908.78 Gt/year for FRIS is used, we obtain a total mean basal melting rate of 1808.3 ± 57 Gt/year. The smaller variability could be explained by the fact that the prescribed melt rates are kept constant, thus the system loses the added variability of FRIS. The PE mean basal mass loss is also smaller with 20.3 Gt/year than just the difference between the PE FRIS and RE FRIS melting rates.

For the extended RE dataset (1980-2059 period) the total mean basal melting rate decreases to 1098.8 ± 82 Gt/year, while in the PE case the values decrease to 1786.2 ± 60 Gt/year. These values are equivalent to a yearly loss of 0.74 meters/year, respectively 1.21 meters/year.

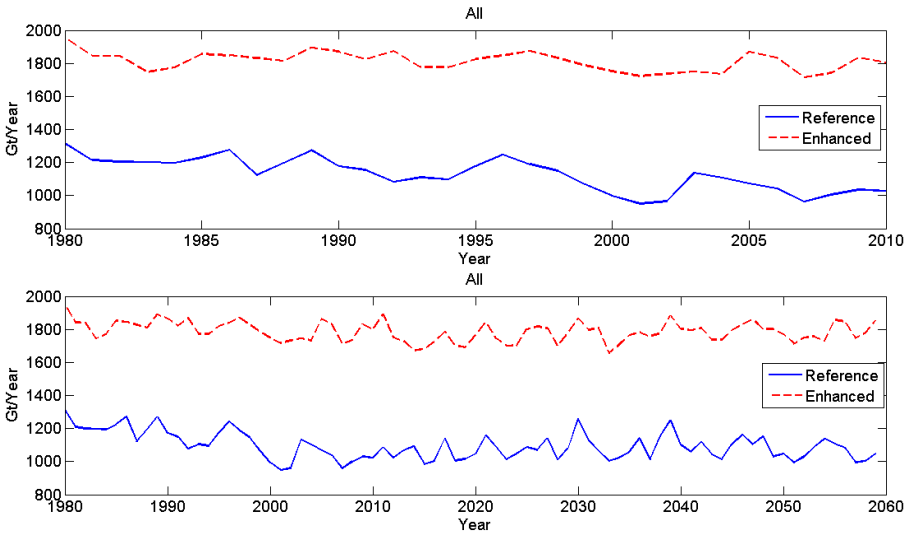

Figure 11: Annual basal melting rate (Gt/year) for all the Antarctic ice shelves, for 1980-2010 period (top panel), and for 1980-2059 (lower panel) with the reference simulation represented by the solid blue line and the enhanced simulation by the dashed red line

Filchner-Ronne Ice Shelf

The mean basal melting rate computed for FRIS for the 1980-2010 period (Fig. 12) is 204.6 ± 61 Gt/year beeing equal to a loss in average of 0.47 meters/year. Strong melting occurs close to the grounding line and also south of Beckner Island with loses of 2-3 me-

ters/year while at the base of Support-Force Ice Stream we have 5 meters/year and at the Foundation Ice Stream it reaches 8.1 meters/years. Underneath the ice shelf marine ice is formed east of Korff Ice Rise up to 1.4 meters/year with a larger area north of it with 0.3 meters/year, while north of Henry Ice Rise we get 0.8 meters/year. Another two marine ice forming areas with values of 1.2-1.6 meters/year are at the north eastern tip of the Beckner Island and western side of the ice front of the Ronne Ice Shelf, areas where Ice Shelf Water is flowing out of the cavity.

Compared to S. S. Jacobs and Frolich (1992) which gives 202 Gt/year, I. Joughin (2003) with 83.4 ± 24.8 Gt/year and E. Rignot (2013) with 155 ± 45 Gt/year the model result obtained was over the high end of the estimates. In previous FESOM simulations, melting rates of 138 Gt/year (R. Timmermann, 2012) were obtained for a forced run and 90 Gt/year (R. Timmermann, 2013) for coupled simulation.

For the extended RE dataset, the total mean basal loss decreases to 190.2 ± 51 Gt/year, equivalent to a 0.44 meters/year loss.

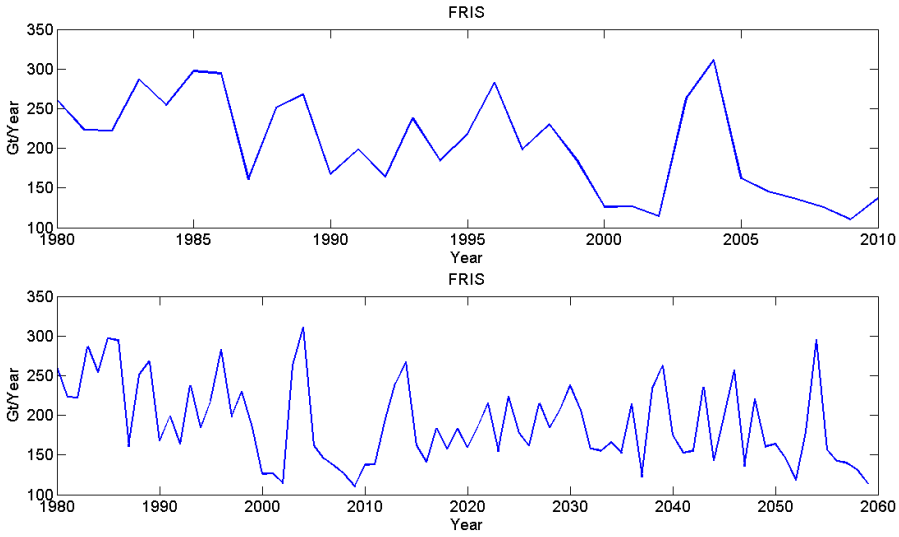

Figure 12: Annual basal melting rate (Gt/year) of the Filchner-Ronne Ice Shelf in the reference simulation, for 1980-2010 period (upper panel), and for 1980-2059 period (lower panel)

Larsen C Ice Shelf

The Larsen C Ice Shelf (Fig.13) which has a high basal mass loss in RE, 85.8 ± 24 Gt/year, sustains a significant decrease in the PE simulation, to 59.4 ± 28 Gt/year. Just two of the 31 years of data have results where the PE has higher values than RE. The pattern continues also in the extended data set with the mean basal mass lose change from 79 ± 25 Gt/year to 47.7 ± 25 Gt/year translating into a loss of 1.7 meters/year to 1.1 meters/year. Maximum values of 7 meters/year are attained in the southern part of the shelf where the ice reaches

400 meters beneath sea level. In the PE case they decrease to 5 meters/year.

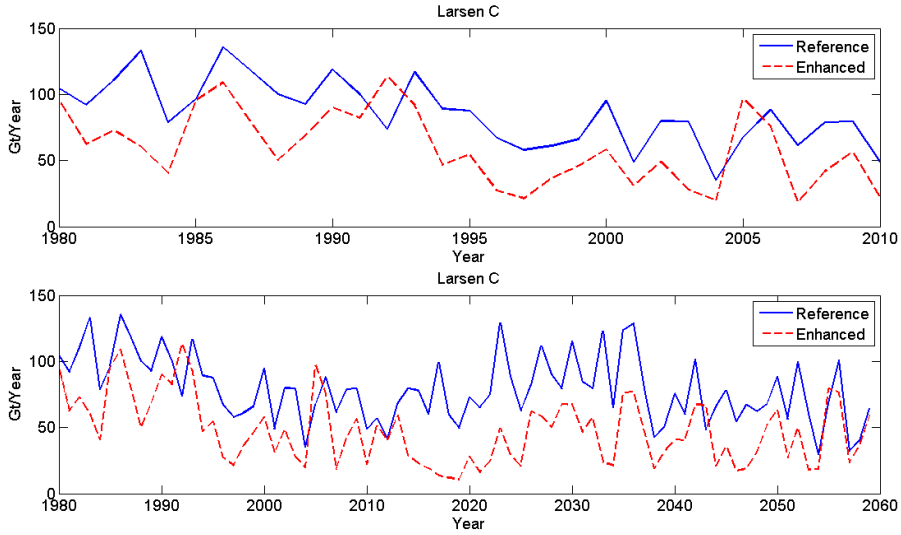

Figure 13: Annual basal melting rate (Gt/year) for the Larsen C Ice Shelf for 1980-2010 period (upper panel), and for 1980-2059 period (lower panel), with the reference run represented by the solid blue line and the enhanced simulation represented by the dashed red line

Eastern Weddell Ice Shelves

The mean melt rate of the Eastern Weddell Ice Shelves (comprised of the Brunt Ice Shelf and Riiser-Larsen Ice Shelf) for RE simulation is 0.75 meters/year (Fig.14) This is well below the 2.3 meters/year estimate done by E. Fahrbach (1994). This is translated into 57.3 ± 22 Gt/year mass loss which is lower than the value obtained by R. Timmermann (2012). The PE simulation shows higher loss 58.2 ± 17 Gt/year but the difference is much smaller than its variability.

Jimbulisen and Jelbart Ice Shelves

The Fimbulisen and Jelbart Ice Shelves (Fig.15) attain a mean mass loss of 56.2 ± 8 Gt/year, while for the PE, the resulting loss is 57.5 ± 7 Gt/year. This values are much smaller than the results from the similar simulationR. Timmermann (2012) which suggested a melting of 130 Gt/year.

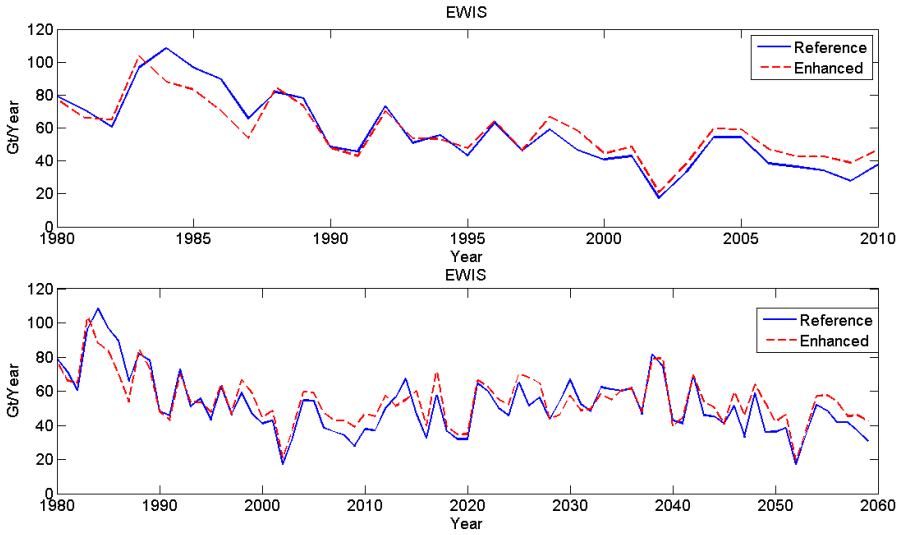

Figure 14: Annual basal melting rate (Gt/year) for Eastern Weddell Ice Shelf, which includes the Brunt Ice Shelf and Riiser-Larse Ice Shelf, for 1980-2010 (upper panel), and for 1980-2059 period (lower panel), with the reference simulation represented by the solid blue line and the enhanced simulation represented by the dashed red line

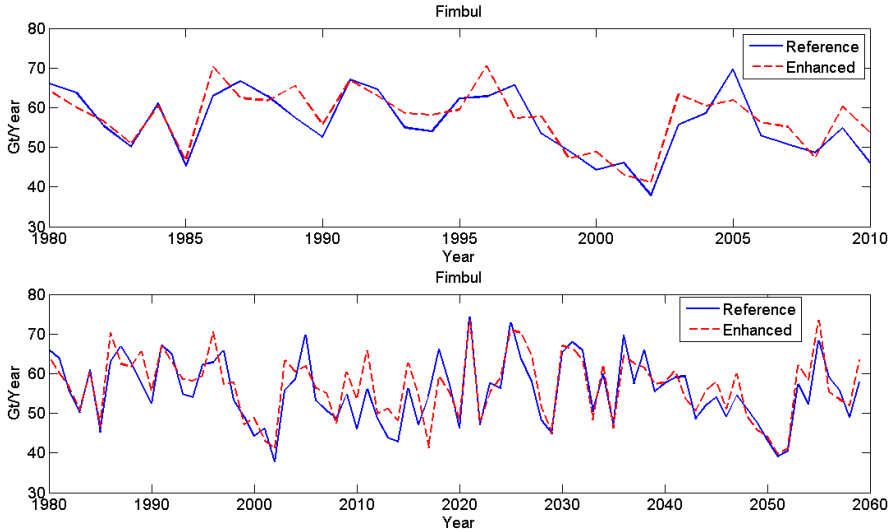

Figure 15: Annual basal melting rate (Gt/year) for the Fimbulisen (and Jelbart) Ice Shelf for 1980-2010 period (upper panel), and for 1980-2059 period (lower panel), with the solid blue line representing the reference simulation and the dashed blue line representing the enhanced simulation

Ice Shelf	Mean Mass Loss ($Gt/year$)	Std ($Gt/year$)	Melt rate ($meters/year$)	Area (km^2)
All	1128.9 1812.7	99 57	-0.76 -1.22	$1477 \cdot 10^3$
FRIS	204.6 908.7	61 -	-0.47 -2.1	$431 \cdot 10^3$
Larsen C	85.8 59.4	24 28	-1.7 -1.17	$50 \cdot 10^3$
EWIS	57.3 58.2	22 17	-0.75 -0.77	$75 \cdot 10^3$
Fimbul	56.2 57.5	8 7.4	-1.1 -1.13	$50 \cdot 10^3$

Table 1: Ice shelves characteristics for 1980-2010 period, where the first row and second row for each ice shelf represents the values for the RE simulation, respectively PE simulation, and All represents all the ice shelves in Antarctica included in the simulation

Ice Shelf	Mean Mass Loss ($Gt/year$)	Std ($Gt/year$)	Melt rate ($meters/year$)	Area (km^2)
All	1098.79 1790.6	82 60	-0.74 -1.21	$1477 \cdot 10^3$
FRIS	190.2 908.7	51 -	-0.44 -2.1	$431 \cdot 10^3$
Larsen C	79 47.7	25 25	-1.56 -0.94	$50 \cdot 10^3$
EWIS	52.2 54.8	17 14	-0.69 -0.72	$75 \cdot 10^3$
Fimbul	55.5 56.8	8 8	-1.09 -1.11	$50 \cdot 10^3$

Table 2: Ice shelves characteristics for 1980-2059 period, where the first row and second row for each ice shelf represents the values for the RE simulation, respectively PE simulation, and All represents all the ice shelves in Antarctica included in the simulation

3.2 Freshwater tracer

The passive freshwater tracer in this simulation is a unitless representation of the quantity of freshwater released at the ice-ocean interface. Everyday the values at the boundary layer are restored to 1. This tracer is used to track the flow of the released meltwater from the ice shelf into the ocean.

By looking at the bottom layer spread of the tracer, we first observed that after 1 month just a small quantity of fresh water reached the bottom at the north east edge of the Berkner Island for the RE and none for the PE. This difference could be explained that the PE has constant release of freshwater while for the RE case the melting can have a high variability. After six months as can be seen in Fig.16 most of the bottom area under the ice shelf, south of Berkner Island, between Korff and Henry Ice Rises and north of them has had contact with the melt water for RE, while for PE we have more tracer in front of the Berkner Island, in the Ronne Basin and further north along the Antarctic Peninsula until 71°S.

(a) Reference (b) Enhanced

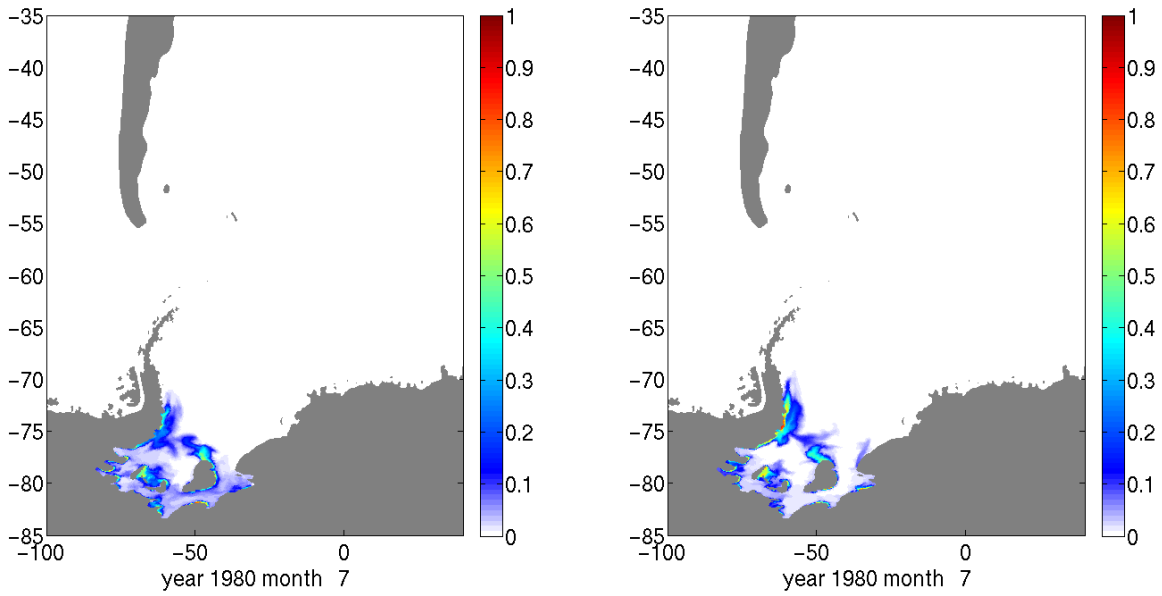

Figure 16: Bottom meltwater tracer in the reference simulation (left) and in the enhanced simulation (right) after 6 months, the colors represent concentration of the tracer that has been released at the ice shelf-ocean interface, with the ice-ocen boundary tracer concetration beeing globally restored to 1

After 5 years (Fig.17) the tracer already occupies the Berkner and General Belgrano Banks in front of the ice shelve but is stopped at the continental slope due to the slope front currents which mainly move all the tracer towards the Antarctic Peninsula. In both cases the tracer reached and filled the Powell Basin north of the peninsula and went around the

South Orkney Plateau through the Jane basin. Here it is slip into two flows, one towards the east along the southern side of the Bruce Ridge and one directly to the north.

(a) Reference (b) Enhanced

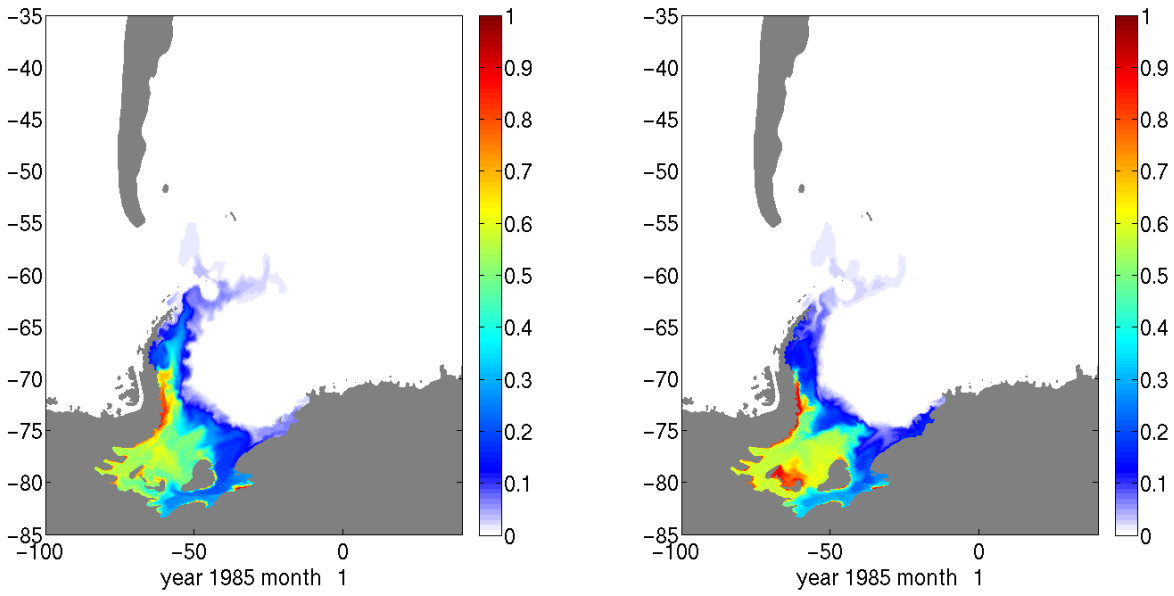

Figure 17: As in Figure 16, but after 5 years of simulation

After 10 years (Fig.18), in the RE simulation the traser is less present at the bottom layer underneath the ice shelf but has extended east along the Bruce Ridge and then filled the South Sandwich Trench and moved north ending in the Georgia Basin. While for the PE simulation, more tracer has accumulated under the ice shelf, but less was transported north, with no tracer being found north of South Orkney Plateau.

After 20 years (Fig.19), in both cases the tracer fills the Hesperides Trough north of the Powell Basin and now has a direct route north from here. For RE, the tracer started spreading in the Argentine Basin, while in the PE case the tracer managed to take the eastern route through the trench.

After 25 years the tracer in the RE simulation manages to fill the South Shetland Through and move south along the peninsula, while in the PE simulation the tracer takes the Bransfield Straight adjacent to the peninsula.

At the end of the simulation the tracer in both cases filled most of the Argentine Basin, flowed towards west, south of the Mid-Atlantic Ridge and managed to spread westwards through the Drake Passage. One the eastern side of the Weddell Sea, the PE tracer moves extremely close to coast towards the east, while the RE tracer is always kept away by the

(a) Reference

(b) Enhanced

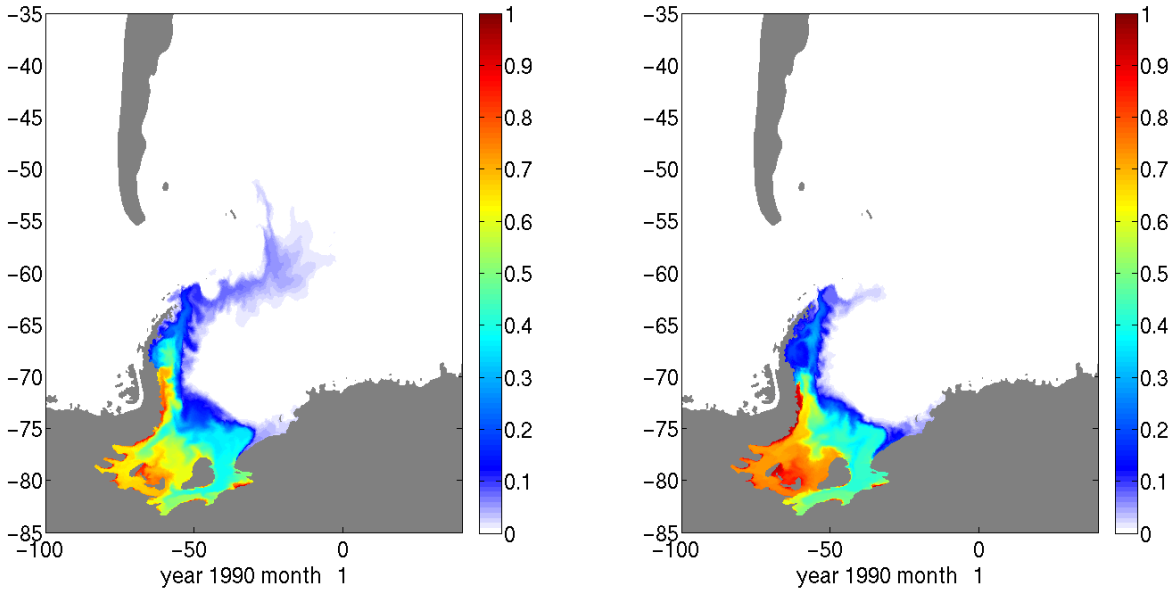

Figure 18: As in Figure 16, but after 10 years of simulation

(a) Reference

(b) Enhanced

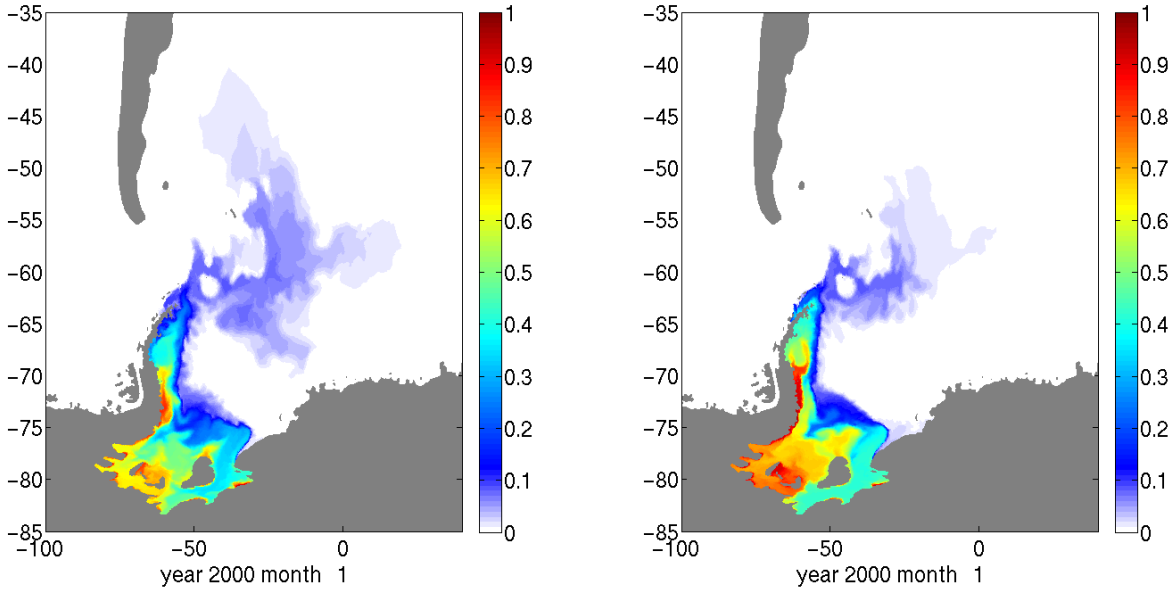

Figure 19: As in Figure 16, but after 20 years of simulation

(a) Reference (b) Enhanced

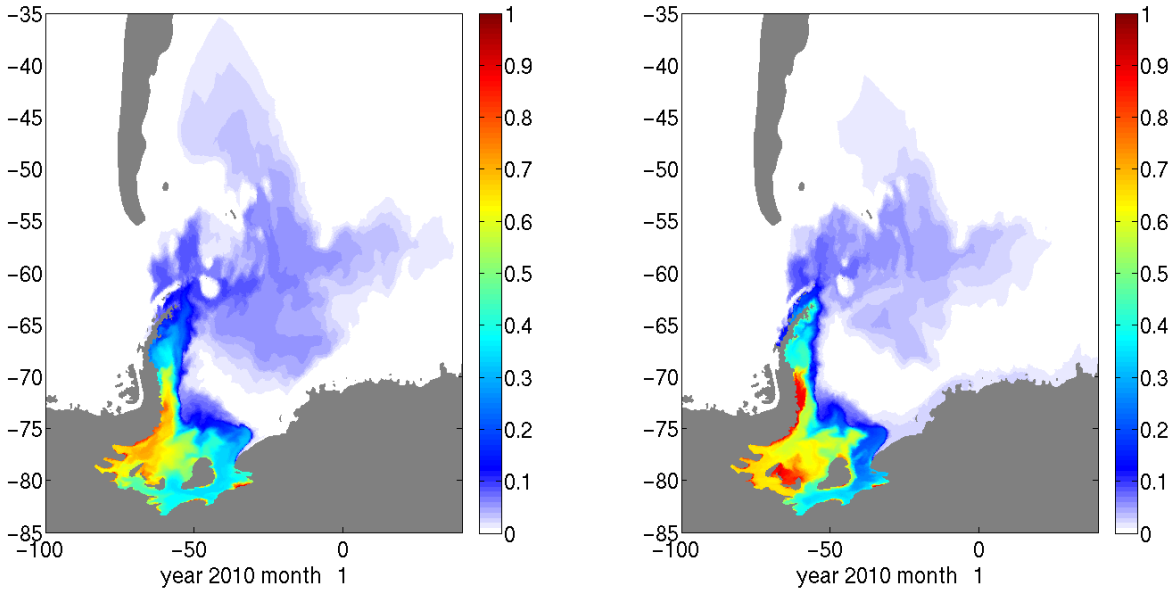

Figure 20: As in Figure 16, but after 30 years of simulation

costal currents as best seen in Fig.21.

(a) Reference (b) Enhanced

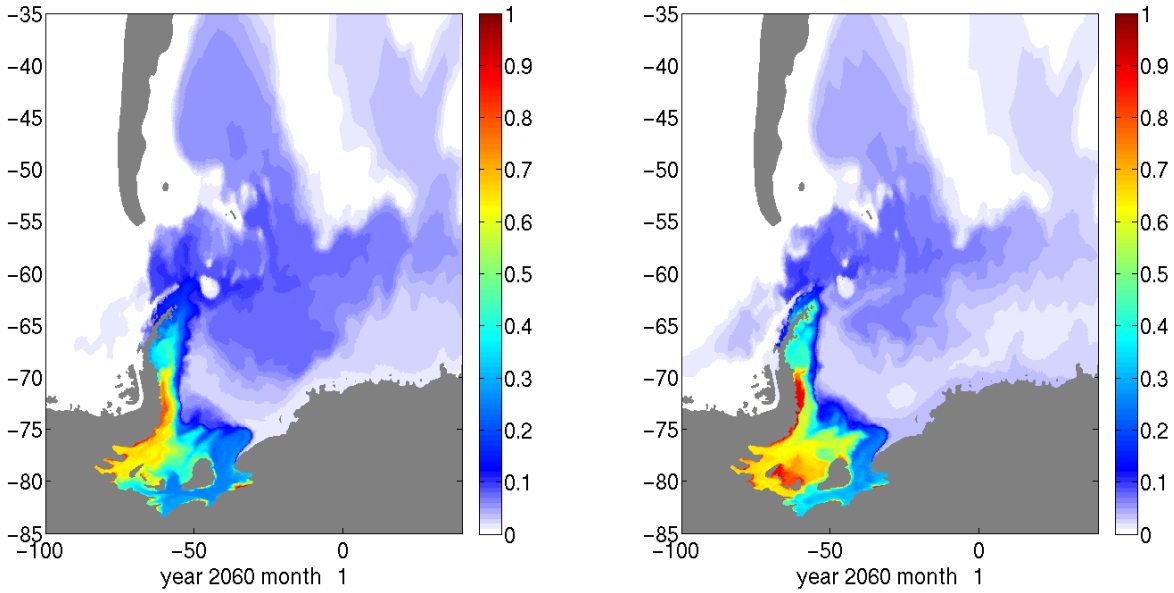

Figure 21: As in Figure 16, but after 80 years of simulation

(a) Reference (b) Enhanced

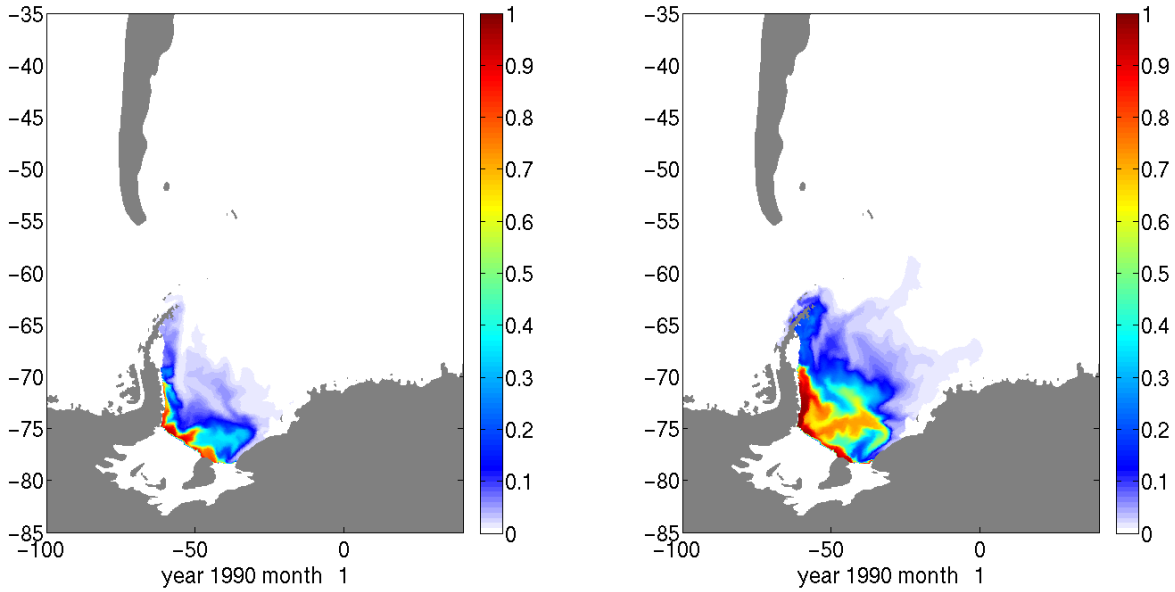

Figure 22: Surface layer freshwater tracer in the reference simulation (left) and in the enhanced simulation (right) after 10 years

The freshwater tracer at the surface, for the PE case, quickly spreads north along the peninsula reaching the tip in 2 years. On the east side of the Weddell Sea the tracer arrives at the Brunt Ice Shelf after 3 years. The tracer passes the Greenwich meridian after 13 years. In the RE simulation the tracer is mostly confined in the Weddell Sea, and needs 10 years necessary to reach the tip of the Antarctic Peninsula.

For the surface, the freshwater tracer is confined in the Weddell Sea in the case of the RE compared to the PE were it leaves the Weddell Sea after approximately 13 years moving eastwards.

In Fig.24 we observe that in the RE case (upper panel) we have represented the strong freshwater flux that exits the cavity on the west side along the peninsula. On the east side we have a second transport of freshwater exiting the cavity on the east side of the Berkner Island and through the Filchner Trough and an inflow of costal waters at the boundary between the continental shelf and Coats Land. In the PE case, the western side transport of freshwater is even stronger but the maximum value of the tracer doesn't reach as low as the RE case. While on the eastern side we have tracer outflowing through the eastern side of the Filchner Through while in the area with costal water inflow the presence of the tracer is even lower than in the RE case.

In fig.25, for the RE case the traser remains confined to the Antarctic Peninsula continen-

(a) Reference (b) Enhanced

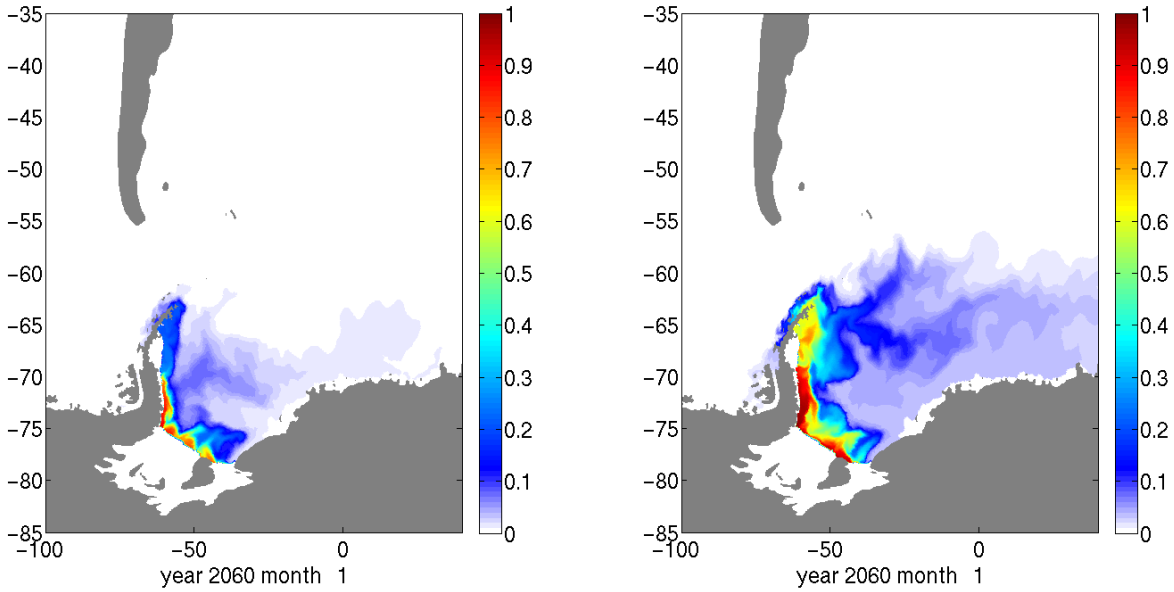

Figure 23: As in Figure 22, but after 80 years of simulation

tal shelf and along the continental slope. For the PE case we observe that beside the west end of the section that shows the freshwater transport towards the north, we also observe the presence of the tracer in the surface layers of the slope region and Weddell Abbysal Plain.

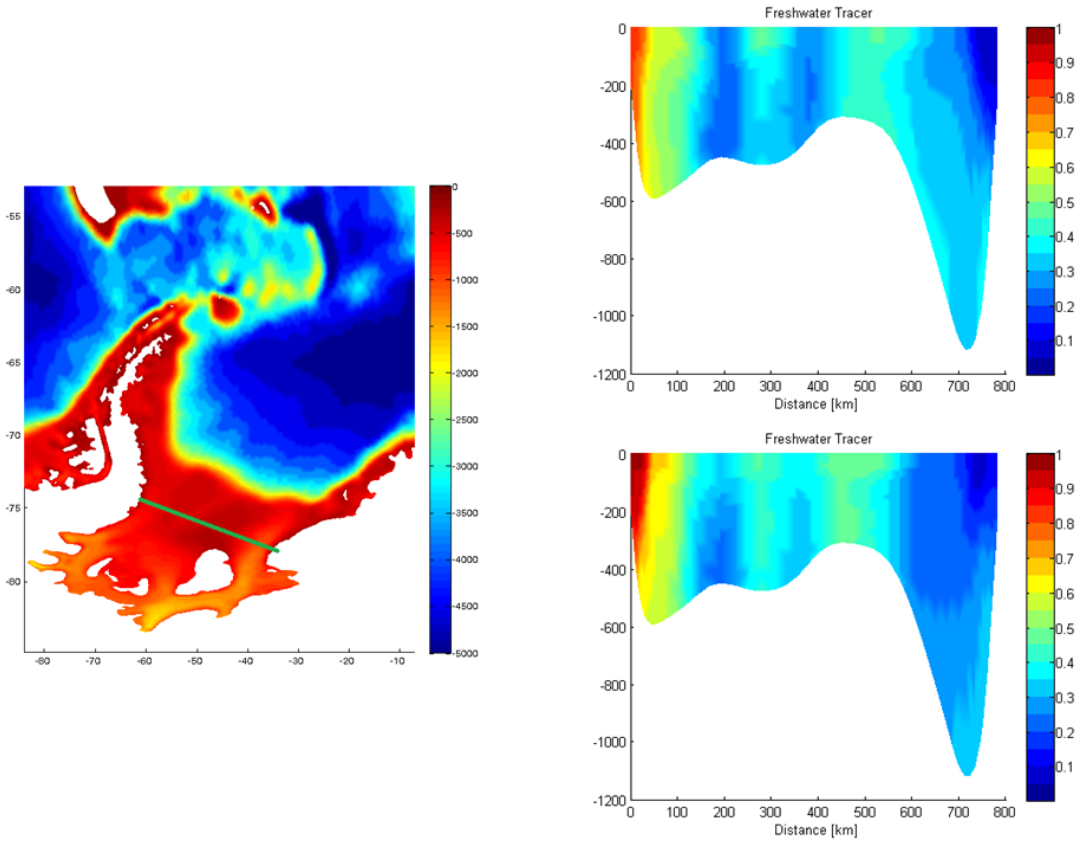

Figure 24: Mean Freshwater tracer sections in front of the Filchner-Ronne Ice Shelf for 1980-1989 period; (left panel) representing the section on the topographical map; (upper panel) RE simulation; (lower panel) PE simulation

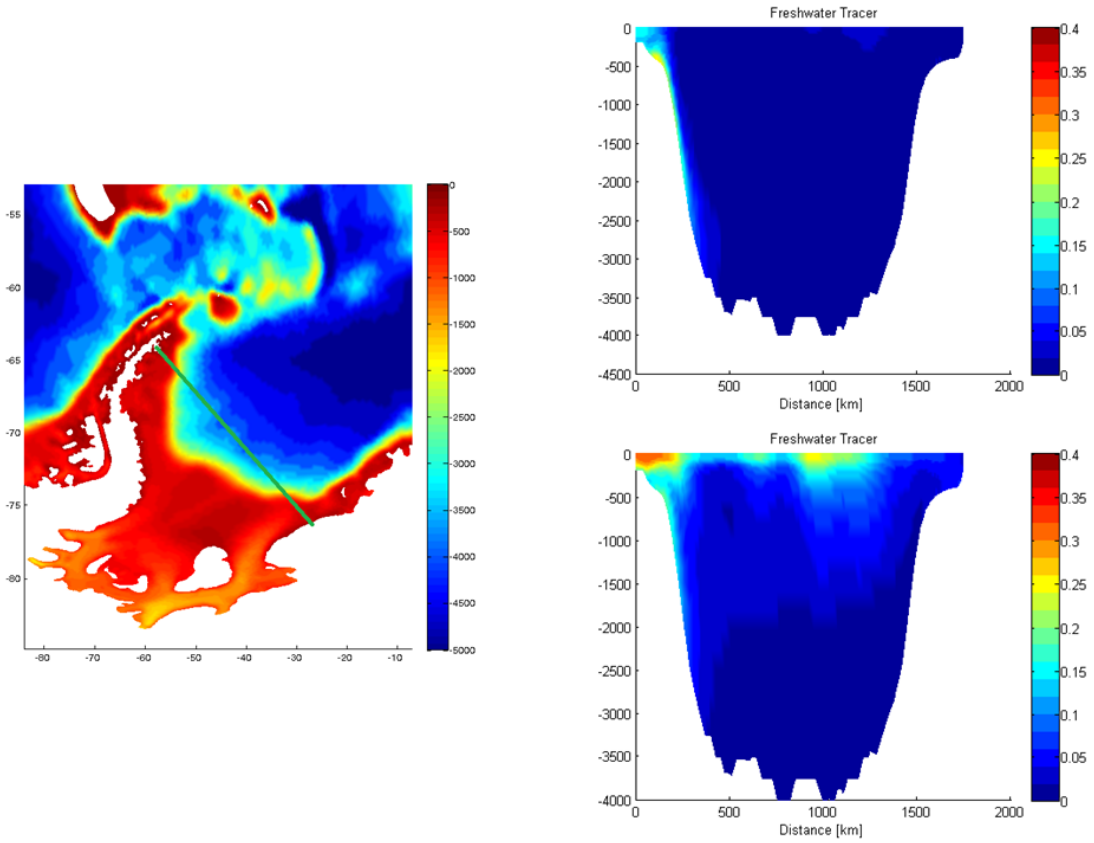

Figure 25: Mean Freshwater tracer sections from the tip of the Antarctic Peninsula to the southern end of the Brunt Ice Shelf for 2000-2009 period; (left panel) representing the section on the topographical map; (upper panel) RE simulation; (lower panel) PE simulation

3.3 Temperature and salinity

Simulated mean bottom water temperatures for RE, during 1980-2010 period in the Weddell Sea sector (Fig.26a) show that the bottom is mainly filled with water below the freezing point at approximately -0.9℃. Along the east coast the potential temperature varies between -1.4 and -1.7℃, with the lower temperatures mainly underneath the ice shelves. Along the peninsula where the main outflow of freshwater exits the cavity, the temperatures go below -2℃. At the norther tip of the Antarctic Peninsula the bottom water potential temperature has -1.2℃ and continues to decrease on its way east and then north through the South Sandwich Trench until it reaches South Georgia Island at -1℃.

(a) Reference

(b) Difference

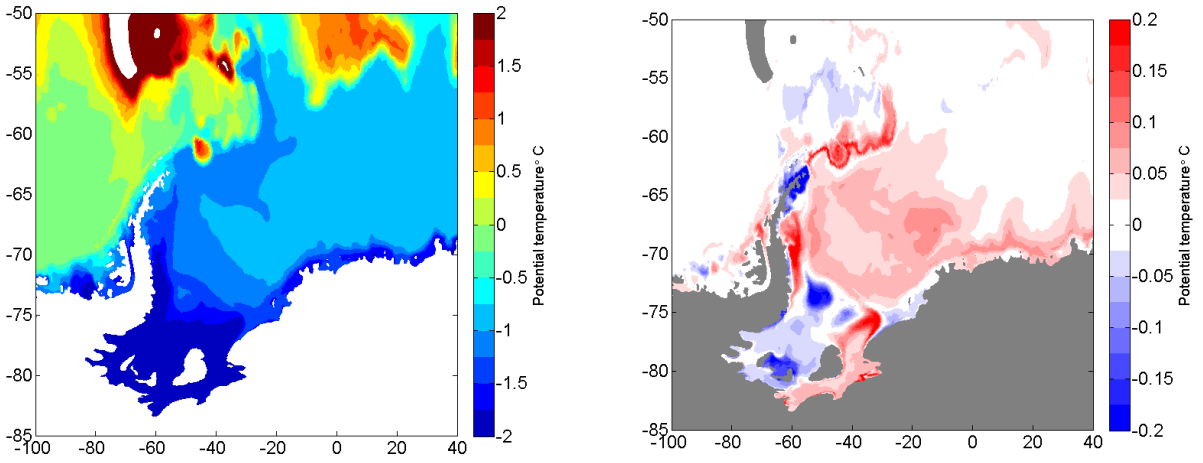

Figure 26: Bottom layer potential temperature mean (℃) for 1980-2010 period; (left) RE case; (right) difference between PE and RE

Underneath the cavity, the potential temperature of the bottom layer in the PE simulation decreases by 0.05℃ east of the Berkner Island, with higher decreases between the Korff and Henry Ice Rises. West and south of the island the potential temperature increases with 0.06℃. In front of the ice shelf we have a strong decrease of 0.2℃ on the General Belgrano Bank. On the eastern side of the continental shelf, an increase of 0.2℃ of bottom water potential temperature is observed at the norther end of the Filchner Trough.At the eastern coast boundary where the coastal currents flow towards the ice shelf there is a small decrease of 0.1℃. The Weddell Sea Abyssal Plain area has a slight increase of 0.06℃ over a large area as it can be seen in Fig.26(b). In the north of the Weddell Sea, following the route that the freshwater tracer takes, we observe an increase in temperature of 0.17℃.

In the 1980-2010 period for the RE experiment, the mean salinity at the bottom of the Weddell Abyssal Plain is in the range of 34.65 to 34.7 PSU as seen in Figure 27a. Underneath

(a) Reference

(b) Difference

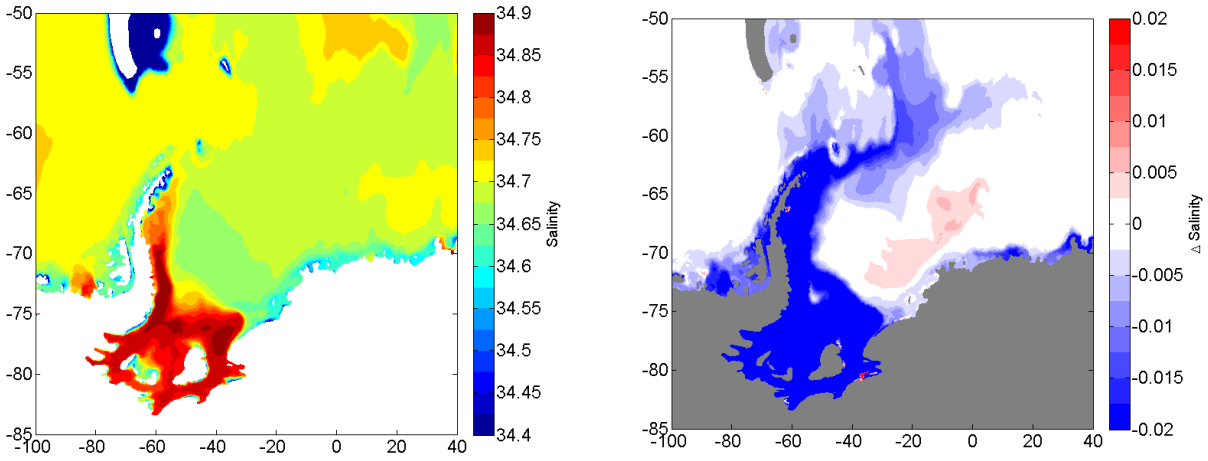

Figure 27: Bottom layer salinity mean for 1980-2010 period; (left) RE case; (right) PE case

the cavity and along the Antarctic Peninsula's eastern coast bottom mean salinity is over 34.8 PSU, with only small regions of smaller than 34.6 psu, mainly areas adjacent to the coast or between the ice rises where freshwater can accumulate. For the PE simulation, the high flux of freshwater decreases salinity at the bottom layer underneath the whole ice shelf, on the continental shelf in front of FRIS and along the peninsula and then east and north until the Georgia Basin. In the Weddell Abyssal Plain there is a small increase of 0.01 PSU at the bottom layer.

3.4 Sea ice

The sea ice extent time series for the Southern Ocean has a representative seasonal cycle (Fig.28). Both september maximum and march minimum are underestimated compared with satellite data. For the RE simulation, the mean September sea ice extent reaches $1.49 \cdot 10^{13}$ m^2, ($2 \cdot 10^{13}$ m^2 for satellite data), and $0.07 \cdot 10^{13}$ m^2 for march (compared to $0.3 \cdot 10^{13}$ m^2). The trend for RE is 3.5% increase per decade (+31.000 km^2/year), while the in the case of PE it decreases to +27.000 km^2/year. The RE sea ice extent increase is over the 1.9 ± 1.3% increase per decade suggested by R. Bintanja (2013).

As it can be seen in Fig.28 the sea ice extent difference between the two simulations (PE - RE) is minimal in the first years of the simulations after the branching. But starting from 1984 until 2000 the difference is mainly positive, while in the 2000-2010 period the mean difference becomes negative. The same happens also for the extended dataset with 2030-2050 being more positive while the 2050-2059 mean difference is slightly negative. This

could point to the fact that the sea ice extent is much more dependent on the atmospheric forcing.

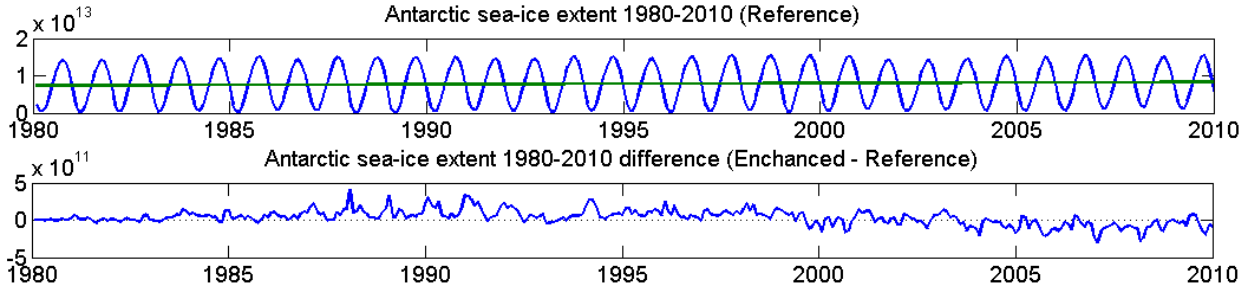

Figure 28: Time series of Antarctic sea ice extent (m^2) in the RE simulation for 1980-2010 period (upper), with the green line representing the trend; and the difference between the PE and RE simulations sea ice extent for the same period (lower)

We defined the Weddell sector as being the area between the Greenwich meridian and 62°W and south of 50°S. In Fig.29 it can be seen that the sea ice extent for the Weddell Sea is higher for PE during the summer minimum (march) with $0.5 \cdot 10^{12}$ m^2 for PE and $0.44 \cdot 10^{12}$ m^2 for RE which represents an increase of 13%. During winter the mean seasonal sea ice extent difference is not significant.

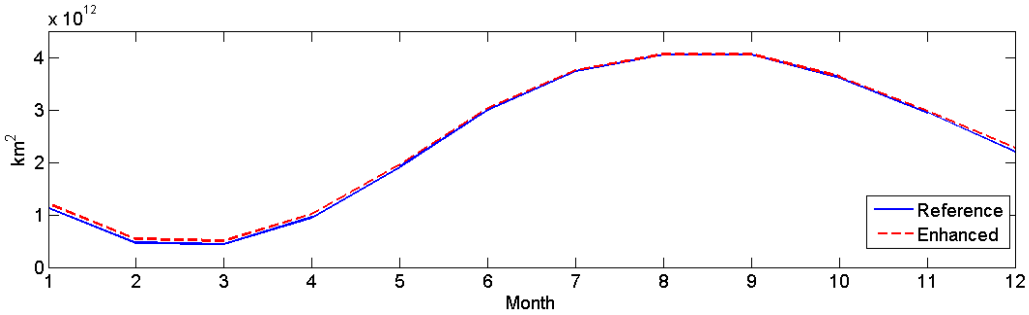

Figure 29: Time series of seasonal mean Weddell Sea sea ice extent (m^2)of the RE simulation (solid blue) and PE simulation (dashed red)for 1980-2010 period

In the case of sea ice volume in the Weddell Sea sector (Fig.30) the changes are more visible. The increase in volume is consistent over the whole year with a maximum difference obtained during the austral winter. For PE simulation in september we obtain the sea ice volume for the Weddell Sea sector of $4.21 \cdot 10^{12}$ m^3 compared to $3.91 \cdot 10^{12}$ m^3 in RE. During the summer minimum the values reach $0.51 \cdot 10^{12}$ m^3 for PE and $0.42 \cdot 10^{12}$ m^3 for RE.

In Fig.31 we observe the sea ice thickness difference between the enhanced run and the reference run for 1980-2010 period. For march which represents the summer sea-ice minimum in the Antarctic, we observe and increase of ice thickness along the Antarctic Peninsula. This area starts close to the Ronne Ice Shelf front and continues until the northern part of the

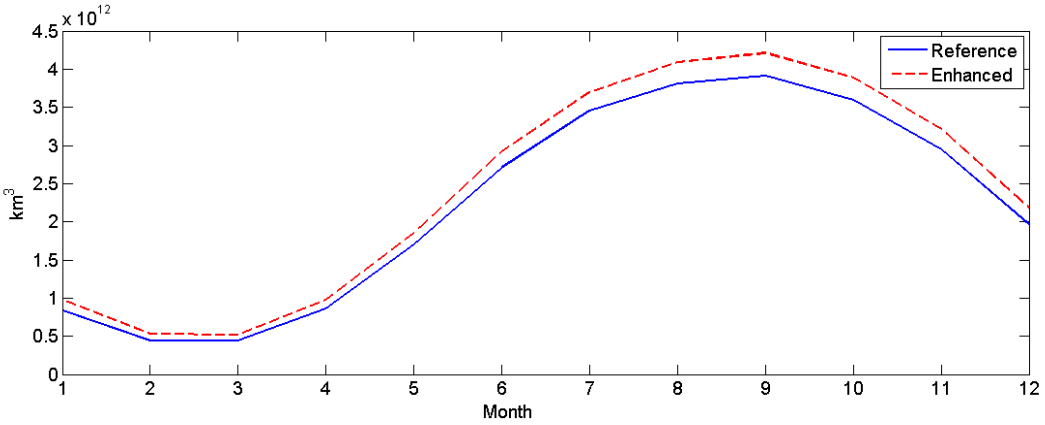

Figure 30: Time series of seasonal mean Weddell Sea sea ice volume for the RE simulation (solid blue) and PE simulation (dashed red) for 1980-2010 period

peninsula, close to the remains of the Larsen A and B ice shelf sectors, with the eastern margin at around 50°W. The Weddell Sea is one of the few areas in the Antarctic where sea ice continues to exist even during the summer. That means that some of the modeled increase represents actual increase in thickness for an area with preexistent sea ice, like south of the Larsen C Ice Shelf, while in front of the shelf itself and further north, it represents the growth of new sea ice. The sea ice thickness also increases towards the middle of the Weddell Sea, above the Weddell Abyssal Plain. The actual thickness increase varies from 0.1-0.2 meters over the abyssal plain to 0.5 meters at the southern edge of the Larsen C Ice Shelf.

In contrast, in front of the Beckner Island and along the eastern coast of the Weddell Sea, sea ice thickness is decreasing. With a maximum decrease of 0.2 meters along the coast and 0.3 meters in front of the island over a larger area, but at the intersection of the island with the ocean and ice shelf there is a strong decrease of 0.55 meters.

For the winter maximum, the increase in sea ice thickness in the Weddell Sea for the PE case is smaller but covers a much larger area. This as see has translated into higher sea ice volume during the austral winter months. Almost all the area in front of the Ronne Ice Shelf until 63°S receives an increase of sea ice thickness between 0.15 and 0.2 meters. Again in north eastern side of the Beckner Island we observe a decrease in thickness. Likewise along the eastern coast of the Weddell Sea.

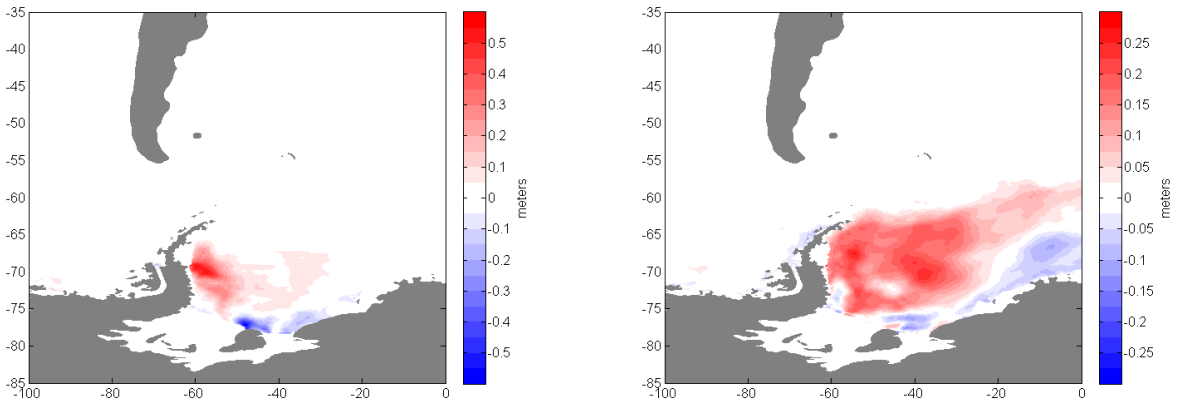

Figure 31: Mean simulated sea ice thickness difference (meters) between the enhanced and reference simulations for the 1980-2010 period; (left) represents the difference during the summer minimum in march; (right) represents the difference during the winter maximum in september

3.5 Meridional overturning circulation and simulated transport

The global meridional circulation forms a strong Antarctic Bottom Water cell, with a mean transport of 16.54 Sv for the RE 1980-2010 period (Fig.32). In the PE case the cell becomes slightly weaker with 16.42 Sv. In the case of the extended data set the, this difference becomes more consistent as seen in Fig.33. In both cases the MOC becomes stronger but the difference between RE and PE increases. For the whole 80 years of data for the RE case the AABW cell reaches a mean transport of 18.25 Sv, while the PE simulation has 17.68 Sv.

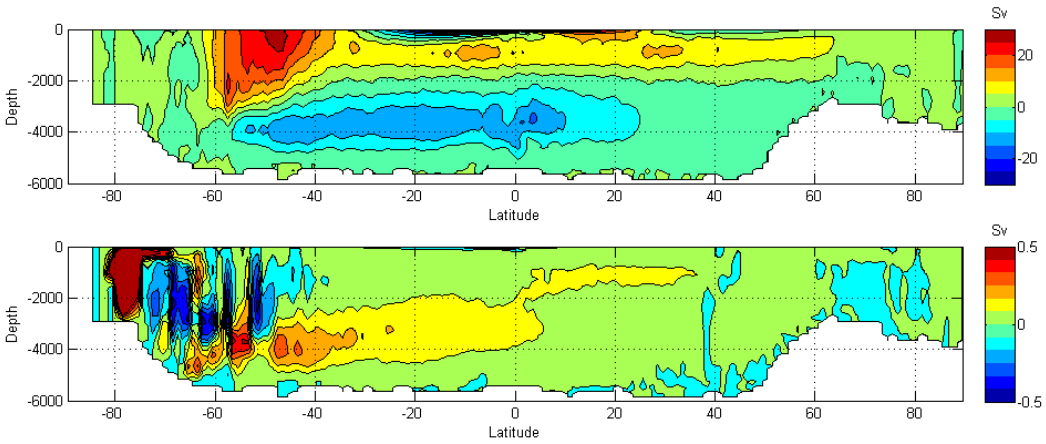

Figure 32: Global meridional overturning circulation for the 1980-2010 period; RE simulation (upper panel) and the difference between the PE simulation and the RE simulation (lower panel)

The AABW cell in the Atlantic sector reaches a mean transport of 3.93 Sv for 1980-2010 (RE) and 3.87 Sv for PE (Fig.34). Again for the extended data set the AABW cell in the Atlantic sector becomes stronger, reaching 5.70 Sv for RE and 5.44 Sv for PE. The changes

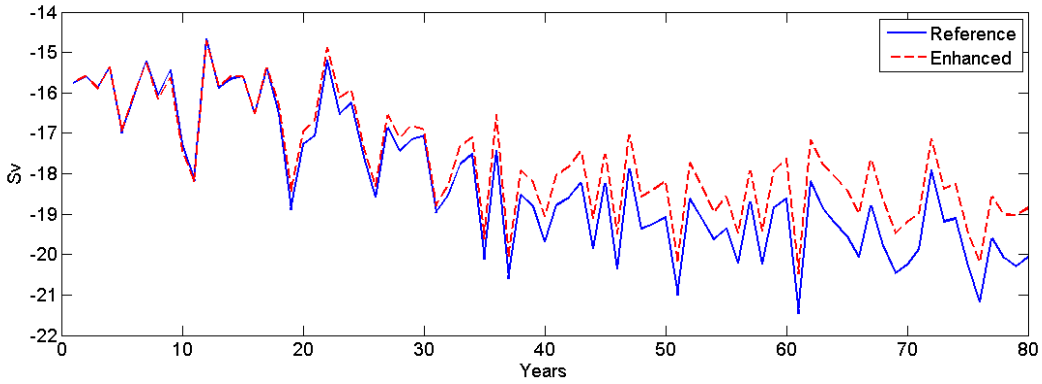

Figure 33: Antarctic Bottom Water MOC cell yearly transport (Sv) for the 1980-2059 period, with the solid blue line representing the RE simulation and the dashed red line representing the PE simulation

in the mean transport in the Atlantic sector for RE represents 96% of the change in AABW cell integrated transport between the first 30 years of data compared to the total of 80 years. The decrease in the AABW cell in the PE simulation is consistent with the increased water freshening of the surface layers which inhibits convection. This leaves more warm water in the deeper layers decreasing the water density.

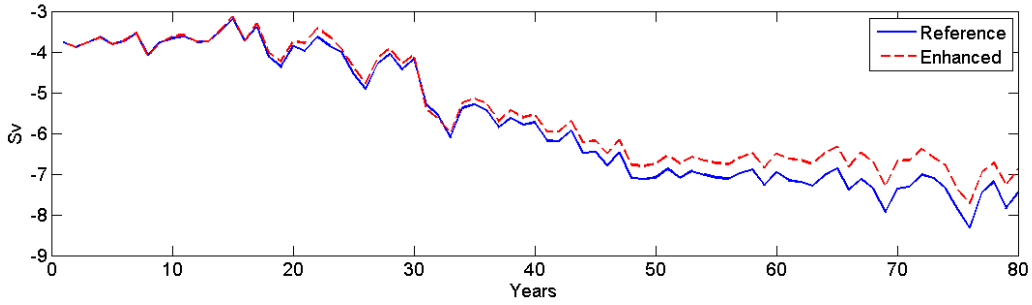

Figure 34: Antarctic Bottom Water Atlantic MOC cell yearly transport (Sv) for the 1980-2059 period, with the solid blue line representing the RE simulation and the dashed red line representing the PE simulation

The yearly average transport in the Weddell Gyre for the first 31 years of integration after the branching is 20.2 Sv which represents just 68% of the 29.5 Sv transport estimated by E. Fahrbach (1994). The PE simulation develops an even smaller transport, 19.31 Sv. As argued for the decrease of the AABW cell transport, the increased water column stability in the Weddell Sea inhibits convection decreasing density at the center of the gyre, reducing its strength (R. Timmermann, 2004). For the 1980-2059 (Fig.36) period the RE run sees an increase in transport in the gyre to 21.65 Sv while in the case of the prescribed melting simulation the transport decreases even more to 18.53 Sv. Just like R. Timmermann (2009) FESOM doesn't manage to reproduce the 60 Sv transport of over the Greenwich meridian. In the first 15 years of the simulations the RE transport has values mostly bigger than in

the PE case. Between 1995 and 2010 in both cases we have an increase in transport and after that the PE case almost always stays has smaller values than RE.

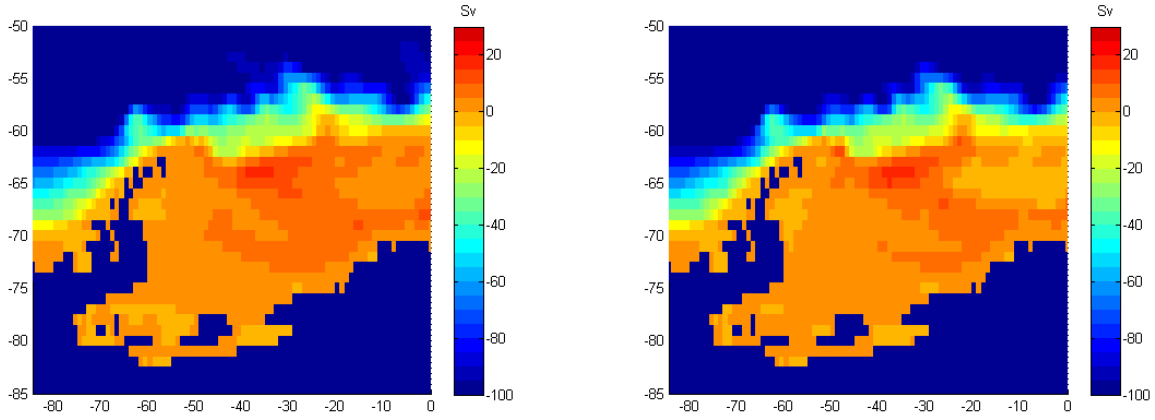

Figure 35: Mean simulated transport stream function (Sv) in the Weddell Sea for the 1980-2010 period; RE simulation (left panel) and PE simulation (right panel)

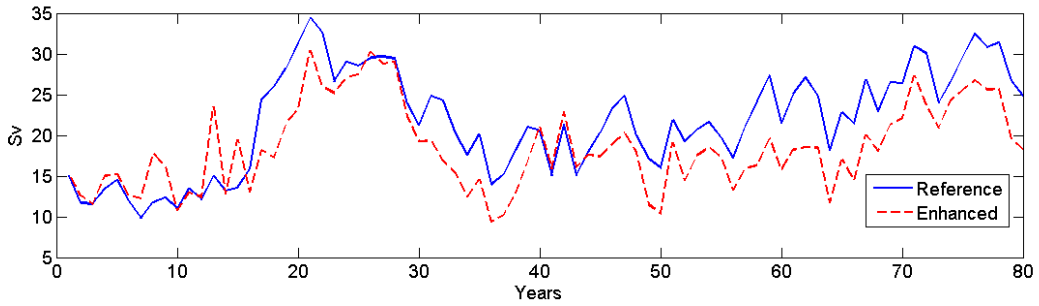

Figure 36: Mean simulated transport (Sv) of the Weddell Gyre for the 1980-2059 period computed for the reference (solid blue) and enhanced simulation (dashed red)

4 Discussion and conclusions

In this study we used the Finite Element Sea-ice Ocean Model to quantify the changes introduced into the sea-ice/ocean system by prescribing increased melt rates for the Filchner-Ronne Ice Shelf. The use of two simulations (reference and enhanced melt rates) that differ from each other in the initial conditions just by the prescription of the melt rates was important for isolating the climate signal of interest.

The results showed that the total melt rate for all the ice shelves is close to observations but melting for the Filchner-Ronne Ice Shelf in the reference simulation is over the upper limit for the first 30 years. The prescribed melt rates in the enhanced experiment are 4 times larger than the mean obtained with present day conditions, and it delivers 50% of the total freshwater in the Antarctic. From this it can be assumed that the results shouldn't be highly influenced by high melt rates in the reference experiment.

The Larsen C Ice Shelf has its basal mass loss overestimated by almost twice relative to the suggested values. It shows a decrease in basal mass loss over time due to the large outflow of freshwater from the Filchner-Ronne Ice Shelf along the Antarctic Peninsula which stabilizes the water column in front of the ice shelf. The the overall temperature in the cavity decreases while the bottom layer temperature increases.

For the Eastern Weddell Ice Shelf we have a small basal mass loss increase in the enhanced simulation which is way below the interannual variability. We do observe a decrease in salinity and temperature in the bottom layer under the ice shelf which could be the result of meltwater from the Filchner-Ronne Ice Shelf entering the cavity but leaves the question open, why there is an increase in melting. In the Fimbulisen Ice Shelf case we also have an increase in melting of almost the same value but here the bottom temperature increases.

The freshwater tracer being a dimensionless measure of melt water release at the ice-ocean interface doesn't give any information about the changes done to the water mass by the freshwater plume. It does show the pathway taken and helps identifying areas where change should exist. The slower advancing tracer in the bottom layer for the enhanced simulation suggests a larger quantity of tracer being kept in the upper layer and at intermediate depths. This freshening over the Weddell Basin protects the deep waters from deep convection thus decreasing the heat loss. The reduced convection in the Weddell basin explains the higher bottom temperatures and higher salinity. This means that less of the Weddell Sea Bottom Water is advected and mixed with the water above thus contributing to the formation of the Antarctic Bottom Water. The increased stability at surface in the center of the Weddell Gyre acts as an inhibitor for downwelling which drives the gyre.

Even if the results are quite realistic, there are a number of issues and weaknesses that if

resolved could improve the accuracy of the data.

The basal melting of the Filchner-Ronne Ice Shelf is dependent on the variability of the sub cavity currents. Prescribing constant melt rates negates the dependence of melting on seasonality, thus reducing the variability of the fresh water flux out of the cavity. The introduction of seasonal variability in the prescribed melting rates could increase the accuracy of localized seasonal effects.

The simulations underestimate the sea ice extent in both summer and winter. As observed in R. Timmermann (2009) study, this deficiency is probably the result of the atmospheric forcing data.

The Antarctic Bottom Water and North Atlantic Deep Water cells are weaker than estimated data. For the AABW we could attribute this mainly to the high basal melting of the Filchner-Ronne Ice Shelf in the reference simulation which changes the water mass properties in the Weddell Sea inhibiting formation of bottom water. For the North Atlantic Deep Water as mentioned in R. Timmermann (2009) one reason could be the insufficient cooling of the Labrador Sea and the rough resolution of the Arctic Ocean.

Most of the smaller shelves in the Antarctic lose mass by calving. Including them in the simulation increased the melt water present in ocean the surrounding the Antarctic changing the local salinity and temperature.

In conclusion, the results presented are in agreement with most known aspects of the ocean/sea-ice system. The climatic signal that appears in the simulation data has physical background. Reducing the number of error sources from the simulations would just increase the accuracy of the results while the general overview of the changes will stay the same.

Bibliography

A. Jenkins David M. Holland. Modeling thermodynamic ice-ocean interactions at the base of an ice shelf. *Journal of Physical Oceanography*, 29:1787 – 1800, 1999.

Carsten Eden Dirk Olbers, Jurgen Willebrand. *Ocean Dynamics*. Springer, 2012.

A. Beckmann E. Fahrbach. *Weddell Sea Circulation, Encyclopedia of Ocean Sciences*. Academic Press, 2001.

M. Schroder V. Strass E. Fahrbach, G. Rohardt. Transport and structure of the weddell gyre. *Annales Geophysicae*, 12:840–855, 1994.

J. Mouginot B. Scheuchl E. Rignot, S. Jacobs. Ice-shelf melting around antarctica. *Science*, 341:266–270, 2013.

M. Morlighem H. Seroussi B. Scheuchl E. Rignot, J. Mouginot. Widespread, rapid grounding line retreat of pine island, thwaites, smith, and kohler glaciers, west antarctica, from 1992 to 2011. *Geophysical Research Letters*, 41:3502–3509, 2014.

Hartmut H. Hellmer. Impact of antarctic ice shelf basalmelting on sea ice and deep ocean properties. *Geophysical Research Letters*, 31(10), 2004.

R. Timmermann J. Determann J. Rae H.H. Hellmer, F. Kauker. Twenty-first-century warming of a large antarctic ice-shelf cavity by a redirected coastal current. *Nature*, 485:225 – 228, 2012.

B. Medley I. Joughin, B.E. Smith. Marine ice sheet collapse potentially under way for the thwaites glacier basin, west antarctic. *Science*, 344:735–738, 2014.

L. Padman I. Joughin. Melting and freezing beneath filchner-ronne ice shelf,antarctica. *Geophysical Research Letters*, 30, 2003.

B. Scheuchl J. Mouginot, E. Rignot. Sustained increase in ice discharge from the amundsen sea embayment, west antarctica, from 1973 to 2013. *Geophysical Research Letters*, 41: 1576–1584, 2013.

B.L.A. Vermeersen A.M. LeBrocq J.L. Bamber, R.E.M. Riva. Reassessment of the potential sea-level rise from a collapse of the west antarcit ice sheet. *Science*, 324:901–903, 2009.

W. S. B. Paterson K. M. Cuffey. *The Physics of Glaciers*. Elsevier, 2010.

K. Makinson T. Gammelsrod K. W. Nicholls, S. Osterhus. Ice-ocean processes over the continental shelf of the southern weddell sea, antarctica: A review. *Reviews of Geophysics*, 47:RG3003, 2009.

S.S. Drijfhout B. Wouters C.A. Katsman R. Bintanja, G.J. van Oldenborgh. Important role for ocean warming and increased ice-shelf melt in antarctic sea-ice expansion. *Nature Geoscience*, 6:376–379, 2013.

A. Beckmann R. Timmermann. Parameterization of vertical mixingin the weddell sea. *Ocean Modeling*, 6:83–100, 2004.

H.H. Hellmer R. Timmermann. Southern ocean warming and increased ice shelf basal meltingin the twenty-first century and twenty-second centuries based on coupled ice-ocean finite-element modelling. *Ocean Dynamics*, 64:1011–1026, 2013.

H.H. Hellmer R. Timmermann, A. Beckmann. The role of sea ice in the fresh water budget of the weddell sea. *Annals of Glaciology*, 33:419 – 424, 2001.

H.H. Hellmer R. Timmermann, Q. Wang. Ice-shelf basal melting in a global finite-element sea-ice/ice-shelf/ocean model. *Annals of Glaciology*, 53(60):303 – 314, 2012.

J. Schroter C. Boning D. Sidorenko K. Rollenhagen R. Timmermann, S. Danilov. Ocean circulation and sea ice distribution in a finite element global sea ice ocean model. *Ocean Modelling*, 27(34):114 – 129, 2009.

J. Schroter S. Danilov, G. Kivman. A finite-element ocean model: principles and evaluation. *Ocean Modelling*, 6:125–150, 2009.

C.S.M. Doake A. Jenkins S. S. Jacobs, H.H.Helmer and R.M. Frolich. Melting of ice shelves and the mass balance of antarctica. *Journal of Glaciology*, 130:375–387, 1992.

R. B. Alley T. K. Dupont. Assessment of the importance of ice-shelf buttressing to ice-sheet flow. *Geophysical Research Letters*, 32:L04503, 2005.

D. Qin T.F. Stocker. IPCC, 2013: Climate Change 2013: The Physical Science Basis. 2013.